Princeton Plasma Physics Laboratory

PPPL-4057

PPPL-4057

A Solar Cycle Dependence of Nonlinearity in Magnetospheric Activity

Jay R. Johnson and Simon Wing

March 2005

Prepared for the U.S. Department of Energy under Contract DE-AC02-76CH03073.

PPPL Report Disclaimers

Full Legal Disclaimer

Trademark Disclaimer

PPPL Report Availability

This report is posted on the U.S. Department of Energy's Princeton Plasma Physics Laboratory Publications and Reports web site in Fiscal Year 2005. The home page for PPPL Reports and Publications is: http://www.pppl.gov/pub_report/

Office of Scientific and Technical Information (OSTI):

Available electronically at: http://www.osti.gov/bridge.

Available for a processing fee to U.S. Department of Energy and its contractors, in paper from:

U.S. Department of Energy
Office of Scientific and Technical Information
P.O. Box 62
Oak Ridge, TN 37831-0062

Telephone: (865) 576-8401

Fax: (865) 576-5728

E-mail: reports@adonis.osti.gov

National Technical Information Service (NTIS):

This report is available for sale to the general public from:

U.S. Department of Commerce
National Technical Information Service
5285 Port Royal Road
Springfield, VA 22161

Telephone: (800) 553-6847

Fax: (703) 605-6900

Email: orders@ntis.fedworld.gov

Online ordering: http://www.ntis.gov/ordering.htm

Accepted for publication in *J. Geophys. Res.*.

A Solar Cycle Dependence of Nonlinearity in Magnetospheric Activity

Jay R. Johnson

Princeton University, Plasma Physics Laboratory, Princeton, NJ

Simon Wing

Johns Hopkins University, Applied Physics Laboratory, Laurel, MD

Abstract. The nonlinear dependencies inherent to the historical K_p data stream (1932-2003) are examined using mutual information and cumulant based cost as discriminating statistics. The discriminating statistics are compared with surrogate data streams that are constructed using the corrected amplitude adjustment Fourier transform (CAAFT) method and capture the linear properties of the original K_p data. Differences are regularly seen in the discriminating statistics a few years prior to solar minima, while no differences are apparent at the time of solar maximum. These results suggest that the dynamics of the magnetosphere tend to be more linear at solar maximum than at solar minimum. The strong nonlinear dependencies tend to peak on a timescale around 40-50 hours and are statistically significant up to one week. Because the solar wind driver variables, VB_s and dynamical pressure exhibit a much shorter decorrelation time for nonlinearities the results seem to indicate that the nonlinearity is related to internal magnetospheric dynamics. Moreover, the timescales for the nonlinearity seem to be on the same order as that for storm/ring current relaxation. We suggest that the strong solar wind driving that occurs around solar maximum dominates the magnetospheric dynamics suppressing the internal magnetospheric nonlinearity. On the other hand, in the descending phase of the solar cycle just prior to solar minimum, when magnetospheric activity is weaker, the dynamics exhibit a significant nonlinear internal magnetospheric response that may be related to increased solar wind speed.

1. Introduction

It is well known that the magnetosphere responds to variation in the solar wind parameters [*Clauer et al.*, 1981; *Baker et al.*, 1983; *Crooker and Gringauz*, 1993; *Papitashvili et al.*, 2000], and it has been established that the magnetosphere has a significant linear response to the solar wind. However, it is also expected that the magnetosphere has a nonlinear behavior due to the internal dynamics associated with loading and unloading of magnetic energy associated with storms and substorms. In this paper, we explore the nonlinear behavior of the magnetosphere as characterized by the planetary index, K_p.

The data analysis of *Bargatze et al.* [1985] indicated that the dynamical response of the magnetosphere to solar wind input could not be entirely understood using linear prediction filters. This finding led to an increasing emphasis on detecting and understanding the nonlinear dynamical behavior of the magnetosphere. A significant body of work focused on trying to characterize magnetospheric dynamics as

a low dimensional chaotic, nonlinear system and focused on calculating properties of a possible strange attractor in the Earth's magnetosphere [*Vassiliadis et al.*, 1990; *Roberts et al.*, 1991; *Roberts*, 1991; *Vassiliadis et al.*, 1991; *Sharma et al.*, 1993]. Many of these studies focused on estimating the dimension of the attractor using such measures as the correlation integral or Taken's estimator [*Takens*, 1980]. Such studies commonly use an embedding based on the time history of a single variable.

The study of *Prichard and Price* [1992] suggested that for datasets with a long autocorrelation time the computation of the correlation integral leads to spurious estimates of the dimension. Moreover, in many cases statistical tests of nonlinearity such as dimension or entropy yield similar results for both the actual dataset and surrogate datasets [*Theiler et al.*, 1992] suggesting that those nonlinear tests do not reveal the presence of nonlinearity on the system [*Prichard and Price*, 1992]. A specific paper addressing the AE index showed no evidence for low dimensional behavior [*Prichard and Price*, 1993]. They argued that it would be appropriate to study the solar wind-magnetosphere interaction as an input-output system rather than as an autonomous system.

Following up on that suggestion, *Price and Prichard* [1993] examined the nonlinear response of the AE index to the VB_s input signal and concluded that there is some evidence for a deterministic nonlinear response of the Earth's magnetosphere. They estimated that consideration of the nonlinearity improved predictive capability by roughly 10%. Improvements in predictive capability using the technique of nonlinear filters [*Vassiliadis et al.*, 1995; *Ukhorskiy et al.*, 2002] and neural networks [*Gleisner and Lundstedt*, 1997] compared with linear predictive filters are also suggestive that nonlinearities in magnetospheric dynamics are important and should be considered for predictive models. That nonlinearity is important in magnetospheric dynamics is also consistent with analysis of physics based magnetospheric analogue models [*Klimas et al.*, 1992, 1994; *Horton and Doxas*, 1996].

In this paper, we apply two discriminating statistical approaches to detect the presence of nonlinearity in magnetospheric dynamics—mutual information and cumulant-based cost. The methods are applied to time series data for K_p. The discriminating statistic basically provides a measure of nonlinear relationships between past and future values of the magnetic indices. Because these measures relate the current state of the magnetospheric index to past values, it provides a measure of predictability for the system.

2. Discriminating Statistics for Linear and Nonlinear Dependencies

It is useful to understand the probability of finding a system in a particular state given past history of the system and/or the past history of the system drivers. We therefore consider a set of input variables $\mathbf{x} \equiv (x_1, x_2, ..., x_n)$, which could consist of past values of the system or data from an external driver, and output variables $\mathbf{y} \equiv (y_1, y_2, ..., y_m)$ for the system. For the magnetospheric system, $\mathbf{x}$ could consist of past history of solar wind drivers such as VB_s and dynamical pressure as well as internal magnetospheric variables such as geomagnetic indices and energetic particle fluxes. The output variables could consist of future geomagnetic indices and particle fluxes.

The standard approach from the theory of linear systems for evaluating the dependencies of the output, $\mathbf{y}$, on the input, $\mathbf{x}$, is to consider the covariance matrix for the variable $\mathbf{z} = (\mathbf{x}, \mathbf{y})$, where the covariance matrix is defined as $\mathbf{C}(\mathbf{z}) = \langle (\mathbf{z} - \langle \mathbf{z} \rangle) \cdot (\mathbf{z} - \langle \mathbf{z} \rangle)^T \rangle$. From the covariance matrix, we can define a measure of the dependency of the output variables on the input variables (e.g. the predictability)

$$\lambda(\mathbf{x}, \mathbf{y}) = \sqrt{1 - \frac{\det(\mathbf{C}(\mathbf{z}))}{\det(\mathbf{C}(\mathbf{x}))\det(\mathbf{C}(\mathbf{y}))}} \qquad (1)$$

which is a generalization of the well known correlation coefficient for one input and one output variable [*Tsonis*, 2001]. It is also obvious that if $\mathbf{x}$ and $\mathbf{y}$ are independent that $\lambda = 0$. On the other hand, if $\mathbf{x}$ and $\mathbf{y}$ are linearly dependent $\det(\mathbf{C}(\mathbf{z}))$ will vanish and $\lambda = 1$.

A more general measure of dependency between an input and output is obtained by considering whether

$$P(\mathbf{x}, \mathbf{y}) \stackrel{?}{=} P(\mathbf{x})P(\mathbf{y}). \qquad (2)$$

where $P(\mathbf{x}, \mathbf{y})$ is the joint probability of $\mathbf{x}$ and $\mathbf{y}$ while $P(\mathbf{x})$ and $P(\mathbf{y})$ are the probability of $\mathbf{x}$ and $\mathbf{y}$ respectively. If the relationship holds, then the variables $\mathbf{x}$ and $\mathbf{y}$ are independent. For all other cases, there is some measure of dependency. In the case where the system output is completely known given the input, $P(\mathbf{x}, \mathbf{y}) = P(\mathbf{x})$. The advantage of considering Equation 2 is that it is possible to detect the presence of higher order nonlinear dependencies between the input and output even in the absence of linear dependencies [*Gershenfeld*, 1998].

In this work, we employ to two discriminating statistics that quantify Eq. 2—mutual information and a cumulant based cost. Mutual information has the advantage that in the limit of Gaussian joint probability distributions, it may be simply related to the linear predictability λ defined earlier [*Li*, 1990]. Cumulants have the advantage of good statistics for limited datasets and noisy systems [*Deco and Schürmann*, 2000]. Moreover, for high-dimensional systems it is more efficient to compute moments of the data rather than try to construct the probability density function.

2.1. Mutual Information

Mutual information (MI) is obtained from entropies, which provide a measure of uncertainty. The mutual information between the input $\mathbf{x}$ and output $\mathbf{y}$ basically compares the uncertainty of measuring a particular input and its output together with the uncertainty of measuring the input and the output independently. Computation of the mutual information involves estimating the probability distribution function using such methods as clustering, kernel density methods or quantization.

For our study, the mutual information is computed as follows: Suppose measurements of two quantities are obtained (e.g. Solar Wind data and K_p measurements or past K_p and future K_p). The datasets will span a range of data which can be binned/quantized—the number of bins may be different if the variables require different resolution. After quantization, we have two variables, x and y, that will take on discrete values, $\hat{x}$ and $\hat{y}$, where

$$\hat{x} \in \{1, ..., N\} \equiv \aleph_1; \hat{y} \in \{1, ..., M\} \equiv \aleph_2 \qquad (3)$$

The variables may be thought of as letters in alphabets $\aleph_1$ and $\aleph_2$ which have N and M letters respectively. The extracted data are then sequences of letters. The entropy associated with each of the variables is defined as

$$H(x) = -\sum_{\aleph_1} p(\hat{x}) \log p(\hat{x}); H(y) = -\sum_{\aleph_2} p(\hat{y}) \log p(\hat{y}); \qquad (4)$$

where $p(\hat{x})$ is the probability of finding letter $\hat{x}$ in the set of x-data and $p(\hat{y})$ is the probability of finding letter $\hat{y}$ in the set of y-data. To examine the relationship between the two variables, we extract a sequence of words $(\hat{x}, \hat{y})$ from the dataset. The joint entropy is defined by

$$H(x, y) = -\sum_{\aleph_1, \aleph_2} p(\hat{x}, \hat{y}) \log p(\hat{x}, \hat{y}); \qquad (5)$$

where $p(\hat{x}, \hat{y})$ is the probability of finding the word $(\hat{x}, \hat{y})$ in the set of (x, y)-data. The mutual information is then defined as

$$I(x, y) = H(x) + H(y) - H(x, y) \qquad (6)$$

Once the data is quantized, computation of the mutual information simply involves sorting the data pairs, counting their occurrence and summing over all possible word combinations.

For a continuous probability distribution, the mutual information is generalized to

$$I(\mathbf{x}, \mathbf{y}) = \int p(\mathbf{x}', \mathbf{y}') \log \frac{p(\mathbf{x}', \mathbf{y}')}{p(\mathbf{x}')p(\mathbf{y}')} d\mathbf{x}' d\mathbf{y}' \qquad (7)$$

In the limit of Gaussian distributed joint probability distribution, the mutual information collapses to

$$I(\mathbf{x}, \mathbf{y}) = \frac{1}{2} \log \left(\frac{\det(\mathbf{C}(\mathbf{z}))}{\det(\mathbf{C}(\mathbf{x})) \det(\mathbf{C}(\mathbf{y}))} \right) \qquad (8)$$

where $\mathbf{z} = (\mathbf{x}, \mathbf{y})$ so that it is natural to define a measure, $\Lambda(\mathbf{x}, \mathbf{y})$ that includes both linear and nonlinear dependency as

$$\Lambda(\mathbf{x}, \mathbf{y}) = \sqrt{1 - e^{-2I(\mathbf{x}, \mathbf{y})}} \qquad (9)$$

[*Li*, 1990; *Darbellay and Vajda*, 1999]. The mutual information may vary from 0 to ∞ so that Λ varies from 0 for independence to 1 for dependence.

The difference between λ and Λ signals the inadequacy of a linear model on the grounds that linear correlations capture only linear relationships. As such, the cost, $D_{MI} = \Lambda - \lambda$ is an indicator of the presence of underlying nonlinear dynamics [*Tsonis*, 2001].

2.2. Cumulant-Based Cost

An alternative measure of the dependency between the input and output is to compute a cost based on evaluating the cumulants of the underlying probability distribution [*Deco and Schürmann*, 2000]. The cumulants may be obtained directly by computing moments from the data and do not require reconstruction of the probability density function.

If Equation 2 were true, then there would be certain statistical relations between the higher-order correlation tensors

$$C_{i...j} = \int d\mathbf{z} P(\mathbf{z}) z_i ... z_j \equiv \langle z_i ... z_j \rangle \qquad (10)$$

where $\mathbf{z} = (\mathbf{x}, \mathbf{y})$ and $i, ..., j \in 1, ..., n+m$ where $\mathbf{x}$ and $\mathbf{y}$ have dimensions n and m respectively. By definition, z_i is an input variable if $i \in \mathcal{M} \equiv [1, n]$ and an output variable if $i \in \mathcal{N} \equiv [n+1, n+m]$. In particular, the cumulants, $K_{1i_2...i_n}$, of the distribution are defined by

$$\begin{aligned} K_i &= C_i = \langle z_i \rangle \\ K_{ij} &= C_{ij} - C_i C_j = \langle z_i z_j \rangle - \langle z_i \rangle \langle z_j \rangle \\ K_{ijk} &= C_{ijk} - C_{ij}C_k - C_{jk}C_i - C_{ik}C_j + 2C_iC_jC_k \\ K_{ijkl} &= C_{ijkl} - C_{ijk}C_l - C_{ijl}C_k - C_{ilk}C_j - C_{ljk}C_i \\ &\quad - C_{ij}C_{kl} - C_{il}C_{kj} - C_{ik}C_{jl} + 2(C_{ij}C_kC_l \\ &\quad + C_{ik}C_jC_l + C_{il}C_jC_k + C_{jk}C_iC_l + C_{jl}C_iC_k \\ &\quad + C_{kl}C_iC_j) - 6C_iC_jC_kC_l \end{aligned} \tag{11}$$

If Equation 2 were true, all cumulants involving cross-correlations between the input and output variables should vanish. Therefore, we define a cost function

$$D_C = \sum_{q=1}^{\infty} \sum_{i_1,...,i_q \in \Pi_q} K^2_{1i_2...i_q} \tag{12}$$

where Π_q are all combinations of q integers $\mathcal{I} \equiv (i_1, ..., i_q)$ such that $\mathcal{I} \notin \mathcal{M}$ or $\mathcal{I} \notin \mathcal{N}$ (that is they are not exclusively input variables or exclusively output variables).

The cumulant-based cost can be used as an indicator of nonlinearity by considering the differences between the cost truncated at second order versus keeping contributions to the cost from higher-order cumulants [*Deco and Schürmann*, 2000]. When the joint probability distribution is Gaussian, all higher order cumulants vanish. It is therefore useful to Gaussianize each input/output variable in computing this discriminating statistic [*Kennel and Isabelle*, 1992; *Schreiber and Schmitz*, 1996; *Deco and Schürmann*, 2000]. The procedure involves (a) drawing a string random data of the same length as the original data set from a Gaussian distribution, (b) ordering the two data sets numerically, and (c) inverting the sorted Gaussian data [as described in *Schreiber and Schmitz*, 1996] according to the inverse map of the original data set. This procedure ensures that higher-order cumulants that are nonzero are only the result of higher-order correlations between the input and output variables and gives a cleaner result.

2.3. Evaluating the Discriminating Statistic

The presence of underlying nonlinear dynamical behavior will be established using the discriminating statistics D_{MI} and D_C. In order to establish the existence of a nonlinearity in the data, we will construct realizations of "surrogate data" [*Theiler et al.*, 1992; *Prichard and Price*, 1992] that share the same linear properties as the original data. In particular, the "surrogate data" have the same autocorrelation, power spectrum, and distribution of values as the original data [*Kugiumtzis*, 1999]. If the discriminating statistic for the original data is significantly different from discriminating statistics of the "surrogate data," then it is unlikely that the original data could be modeled as a linear process such as a simple autoregressive (AR) model. In this way we falsify the "null hypothesis" that the underlying dynamics can be described as a linear process.

The discriminating statistic will be computed for the actual data set, D_0, as well as for N_S surrogate data sets, D_{S_i}, (where S_i is the i^{th} surrogate set). Falsification of the null hypothesis will be gauged by the significance, $S = |D_0 - \mu_S|/\sigma_S$ where $\mu_S \equiv \sum_i D_{S_i}/N_S$ is the average of the statistic over all surrogate data sets and $\sigma_S^2 = \sum (D_{S_i} - \mu_S)^2/(N_S - 1)$ is the variance of the surrogate data. The hypothesis is falsified when the significance exceeds an arbitrary value. A common choice is 2 or 3 standard deviations which gives 95% and 99.5% assuming a normal distribution. The assumption of normal distribution is reasonable when as few as 30 surrogate datasets are used. We have found little difference from the case where as many as 500 surrogate data sets were used.

For the analyses in this paper, we will be considering time series of geomagnetic indices. To prepare the surrogate data, we apply the corrected amplitude adjusted Fourier transform method (CAAFT) [*Kugiumtzis*, 1999]. The generated surrogate data are like the amplitude adjusted Fourier transform method (AAFT) [*Theiler et al.*, 1992], but corrected to match the autocorrelation (necessary due to the limited size of the dataset [*Schreiber and Schmitz*, 1996]). For the correction, a linear interpolation for the graph of the relation between the Gaussian and the transformed autocorrelation is found, for lags up to a given τ_{max}. This τ_{max} will be taken at least as large as the maximum timescale of interest for our calculations. Using this interpolation function, for the autocorrelation of the given time series, the autocorrelation of the respective Gaussian time series is estimated. Based on this autocorrelation, the coefficients of the corresponding AR model of order p (which we prescribe as the length τ_{max}/(number of measurements) are estimated and an AR-time series is generated, and transformed to match the amplitude distribution of

the original time series. This process is performed 20 times to obtain a statistic of candidate AR models. Then the most proper is selected, in the sense that the autocorrelation of the generated surrogate matches best the autocorrelation of original data set. Based on this AR model, we generate realizations of a surrogate data stream and transform to match the amplitude distribution of original data. In our analysis, we find that the linear properties of the data are well captured by this method.

2.4. Significance as an Indicator of Nonstationarity

If it is expected that the underlying dynamics of a system are nonstationary, it is appropriate to test how the significance changes as a function of time. This test may be performed by considering the evolution of the significance computed in overlapping windows as a function of time (a task similar to constructing a spectrogram). If the significance changes appreciably over time, it is a good indicator that the dynamics are changing. Because the cumulant-based statistic has the advantage of good statistics for limited datasets, the technique would be far better than the mutual information based statistic for examining nonstationarity in a dataset on short timescales. In our study, we examine the significance of the underlying magnetospheric dynamics over the history of the K_p which includes nearly seven full solar cycles. We compute the discriminating statistic for each year using three year windows of data which is adequate to resolve changes in the underlying dynamics over the course of an eleven year solar cycle. In order to achieve good statistics using the mutual information based discriminating statistics it was necessary to compute the significance using three year data windows. The use of smaller data windows would degrade the mutual information results so that no meaningful conclusion could be drawn from the analysis. On the other hand, the cumulant based statistic could be reasonably applied to data windows as short as a few days to detect changes in the underlying dynamics.

3. Application to Magnetic Indices

The state of the magnetosphere is commonly designated using the global magnetic activity index, K_p. K indices isolate solar particle and IMF effects on the earth's magnetic field; over a three-hour period, they classify into disturbance levels the range of variation of the more unsettled horizontal field component on the ground. Each activity level relates almost logarithmically to its corresponding disturbance amplitude. Three-hour indices discriminate conservatively between true magnetic field perturbations and the quiet-day variations produced by ionospheric currents. K indices are quantized in 28 steps from 0 (quiet) to 9 (greatly disturbed) with fractional parts expressed with +/- or in thirds of a unit.

Our initial examination of the nonlinearity of the K_p time series suggested a solar cycle dependence in the nonlinearity. In order to achieve better statistics (particularly for the mutual-information measure), we found it useful to consider data from three year windows. This length of window is appropriate for discriminating differences in dynamical behavior over the course of the 11-year solar cycle.

3.1. Mutual-Information Based Predictability

In Figure 1 we show the results from the mutual-information based predictability for data near a solar maximum for the years 1980-1982. Panel (a) shows the linear correlation as a function of time delay. Panel (b) shows the mutual-information based measure of correlation as a function of time delay. Panel (c) shows the difference between (a) and (b) as a function of time delay. The mean and spread of the surrogate data are also shown with dotted and dashed lines respectively. The significance based on panel (c) is shown in panel (d). The open circles indicate that the measure of nonlinearity suggests the measured data was more linear than the surrogates while the crosses indicate when the significance indicates the measured data was more nonlinear than the surrogates. Several items of importance should be noted. First, panel (a) demonstrates that the linear properties of the surrogate datasets are statistically identical to those of the measured data. Second, the nonlinearity measure of the surrogate data increases with time delay. This increase is a result of (a) the limited size of the dataset, (b) the fact that the data is not Gaussian distributed, and (c) the fact that the CAAFT method while preserving linear properties is itself a nonlinear transform which could introduce additional nonlinearities into the data. Third, for this solar maximum the value of the significance is generally less than 1 indicating that there is no statistical difference between the measured data and the surrogate data. Therefore the assumption that the underlying dynamics can be described with a linear AR process based on the last 200 hours of data is not falsified. A second example showing similar results

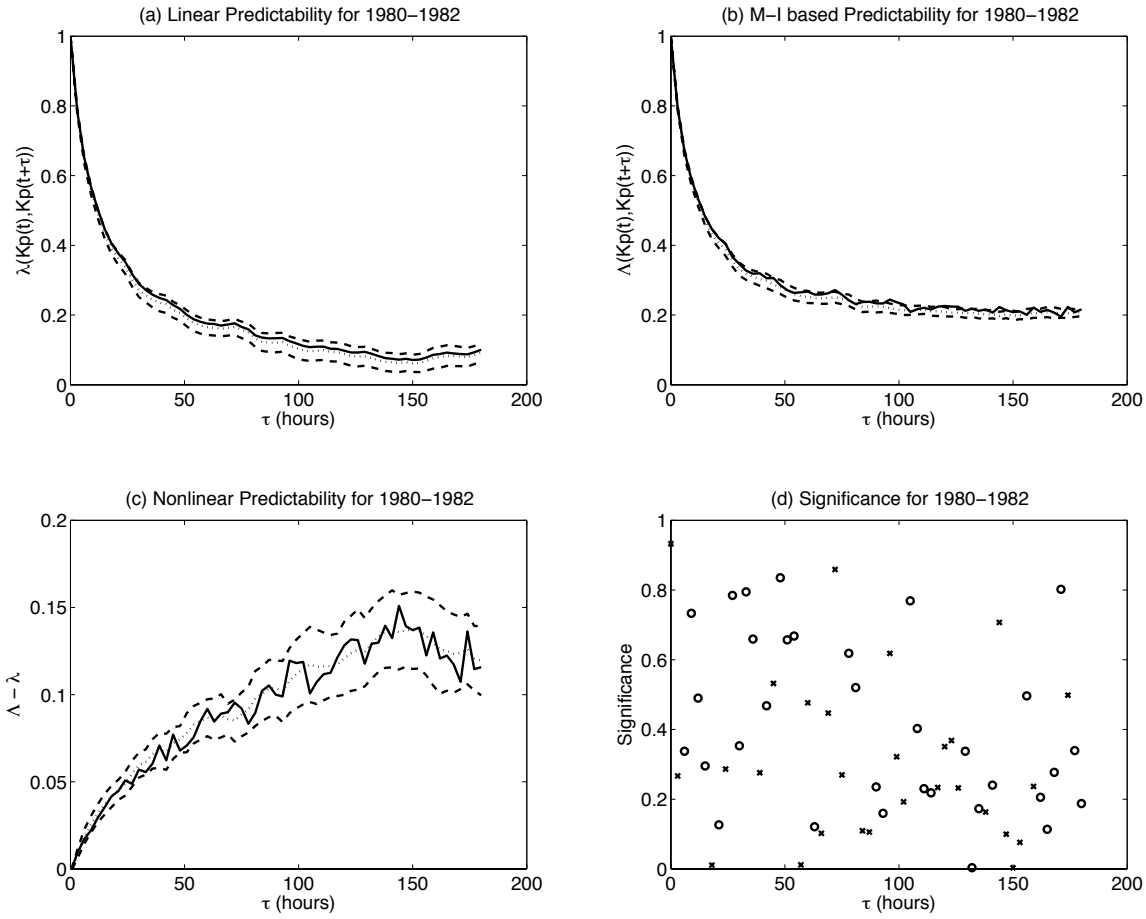

Figure 1. Analysis of K_p data from 1980-1982 (near a solar maximum) using the difference between linear predictability and mutual information based predictability as the discriminating statistic. Panel (a) shows the linear predictability (λ); panel (b) shows the mutual-information based predictability (Λ); panel (c) shows the discriminating statistic ($\Lambda - \lambda$); and panel (d) shows the significance based on panel (c). In all figures, the quantities derived from the actual data are shown as solid lines, the means of the surrogates are shown with dotted lines and the upper and lower standard deviations of the surrogates are shown as dashed lines. Significances that are positive (more nonlinear) are shown as an x while negative (more linear) significances are shown with an o. This analysis suggests that there is no statistical difference between the discriminating statistic for the surrogate data and the actual K_p sequence.

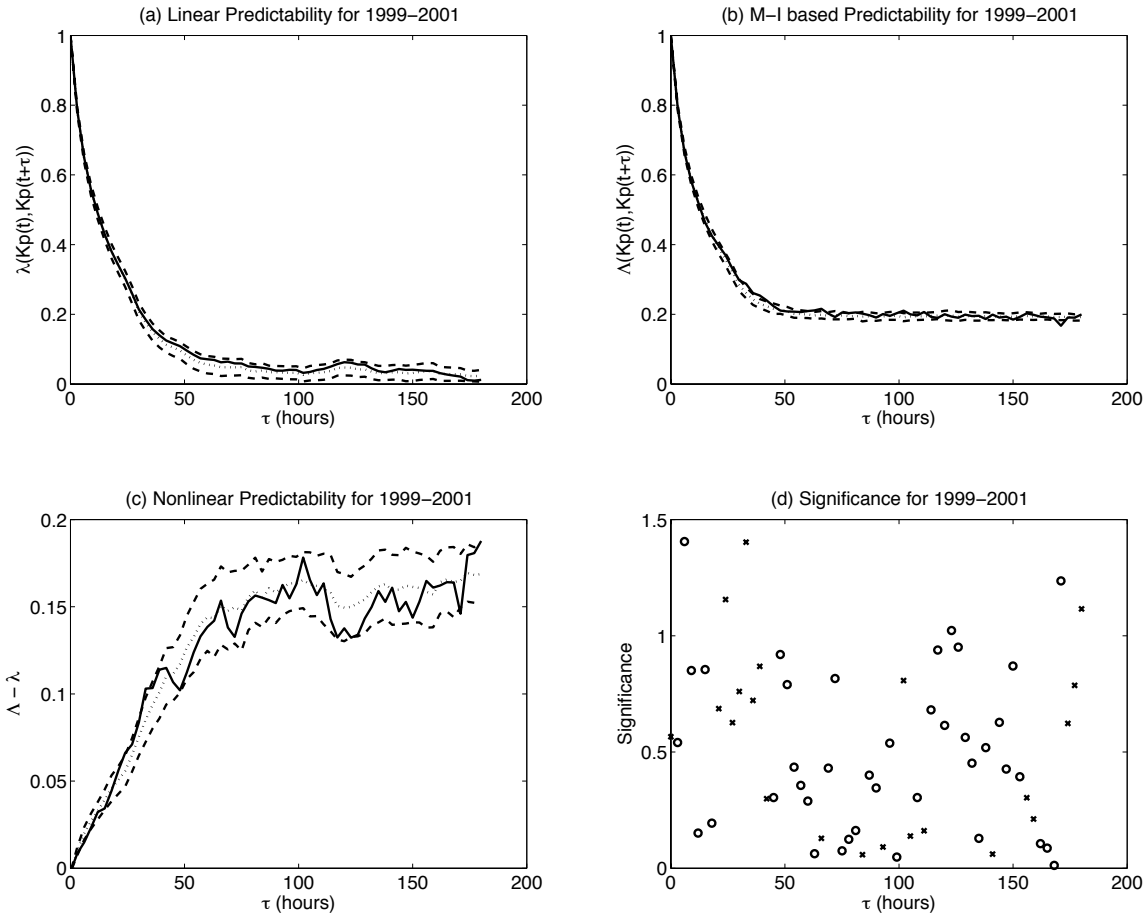

Figure 2. Analysis of K_p data from 1999-2001 (near a solar maximum) using the difference between linear predictability and mutual information based predictability as the discriminating statistic. The format is the same as for Figure 1. Note that as for the 1980-1982 solar maximum, there is no evidence to suggest any difference in the discriminating statistic from the surrogate data which was obtained from the CAAFT method.

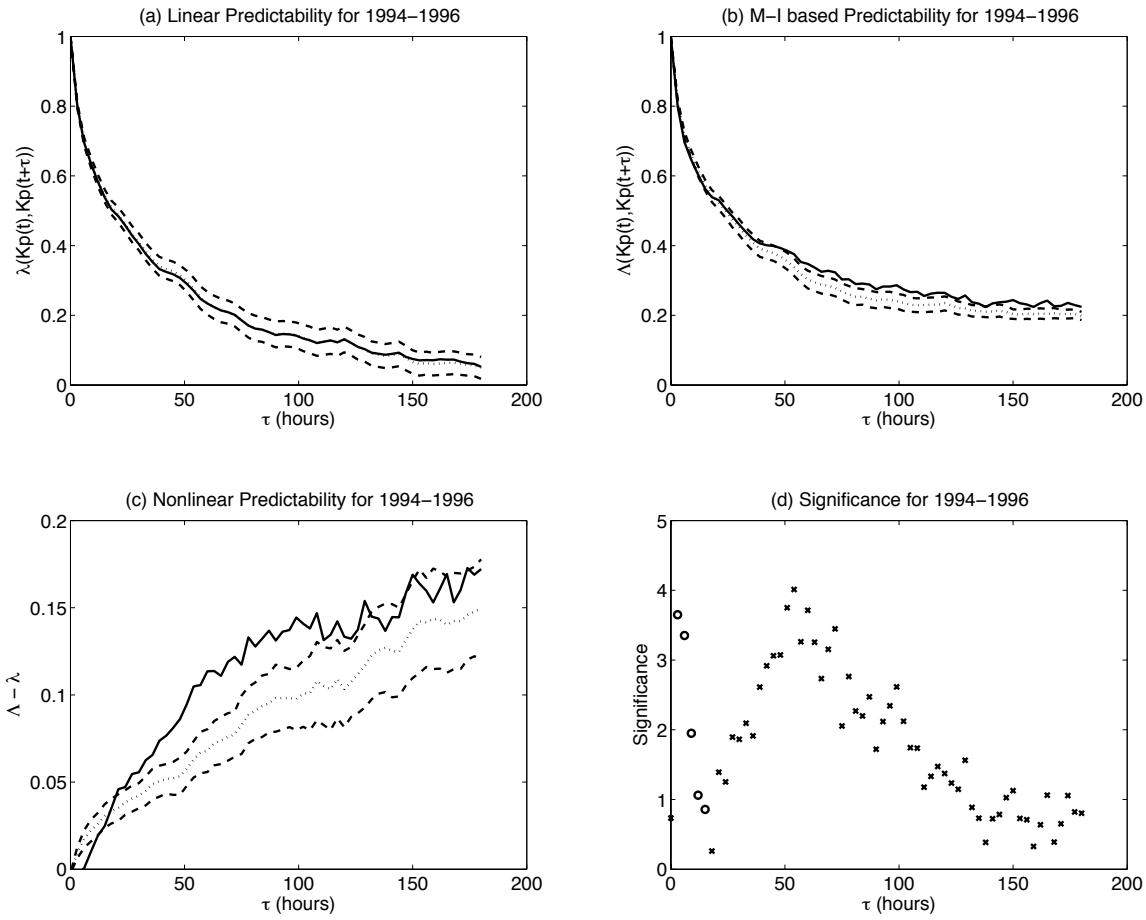

Figure 3. Analysis of K_p data from 1994-1996 (near a solar minimum) using the difference between linear predictability and mutual information based predictability as the discriminating statistic. The format is the same as for Figure 1. Note that although the linear properties of the K_p time series are well reproduced by the surrogates, the discriminating statistics indicate that there is significant nonlinearity that has not been captured. The significance can be as large as 4 standard deviations and peaks around 50 hours.

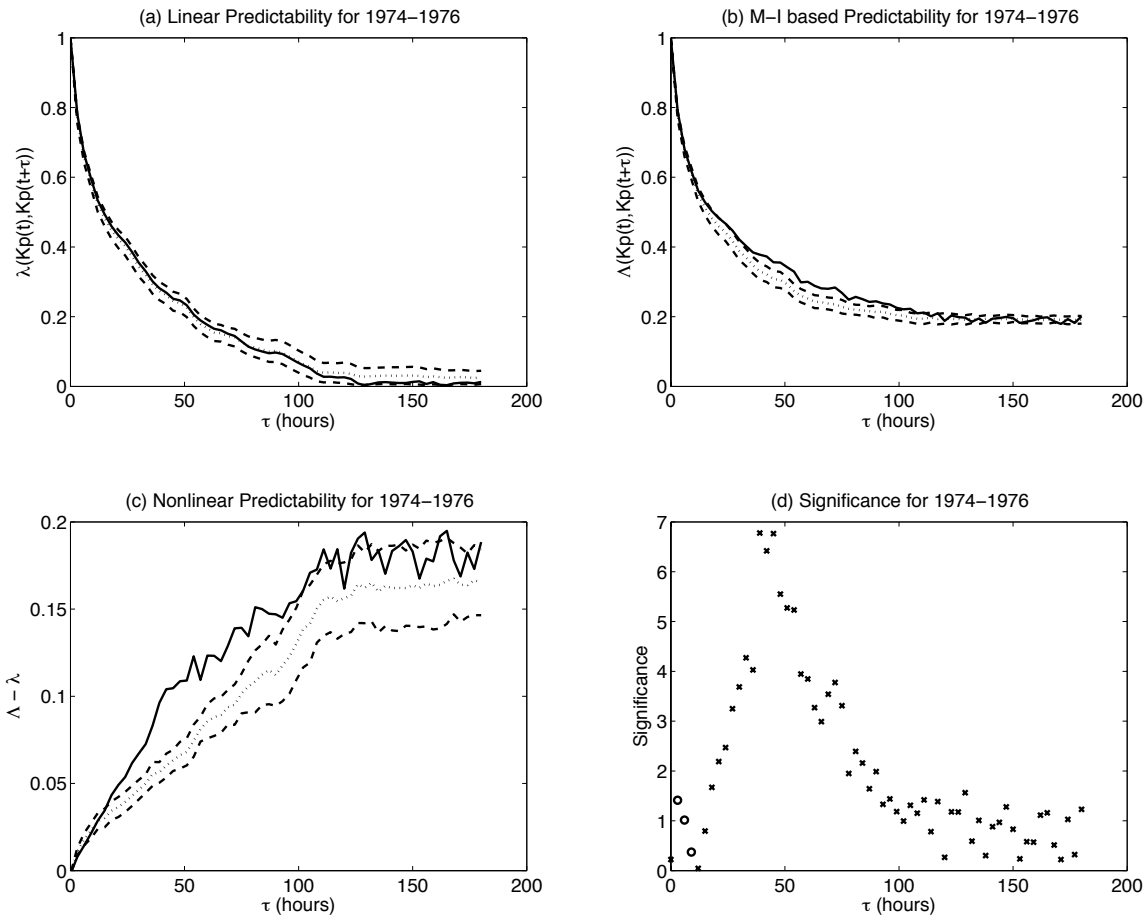

Figure 4. Analysis of K_p data from 1974-1976 (near a solar minimum) using the difference between linear predictability and mutual information based predictability as the discriminating statistic. The results are similar to the analysis of the solar minimum shown in Figure 3.

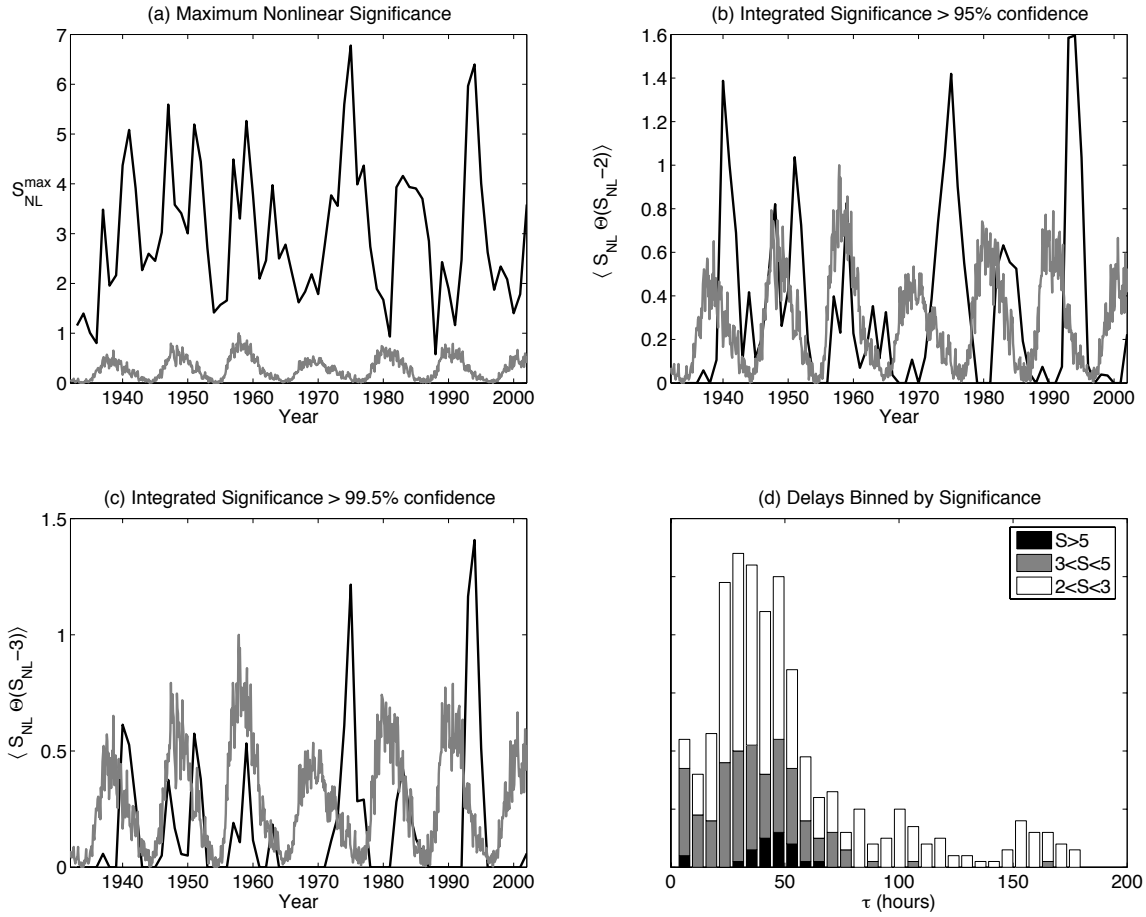

Figure 5. The solar cycle dependence of the mutual-information based significance is shown for the historical K_p timeseries. Panel (a) shows the maximum significance for each 3 year window of data; panel (b) integrates all positive significance larger than 2; panel (c) integrates all positive significance larger than 3; and panel (d) shows a histogram of all significance measures larger than 2 for all historical K_p. The data are grouped into several significance ranges. Statistically, large significance appears to peak around 30-50 hours. When the significance is larger, the peak is tightly clustered around 50 hours. For reference, the sunspot number (scaled for clarity) has been displayed in panels (a)-(c) with a light line. Note that minima in the nonlinearity coincide with maximum sunspot number and the maximum nonlinearity occurs approximately two years before the minimum sunspot number.

for another solar maximum is shown in Figure 2.

For a solar minimum (1994-1996) the results of this analysis are strikingly different as shown in Figure 3. The format of the plots is the same as in Figure 2. While again, the surrogates capture the linear properties of the data, the measure of nonlinearity is significantly different. The significance exceeds 3 for time delays on the order of 40-75 hours falsifying the null hypothesis that the system could be modeled as a linear AR process on those timescales. The negative values for the significance for short delays indicates that the real data behaves more linearly than the surrogate data (but also seems related to the fact that the surrogates do not have much spread at small correlation time). A similar case is shown for another solar minimum in Figure 4 which also indicates a peaked nonlinear significance at a correlation time of 50 hours. It should be noted that the nonlinear peak for 1994-1996 is broader than the more focused peak for 1974-1976 which has very high significance. It should be concluded that there is a significant nonlinearity in the underlying dynamics of the system for these years.

In order to evaluate whether this nonlinear feature is related to the solar cycle, we examined all data available from 1932-2003 using a three year window as in Figures 1-4. The results of this analysis are shown in Figure 5. In this figure we present several measures of nonlinear significance over the course of several solar cycles. Panel (a) shows the maximum significance for each year. Panel (b) shows an integrated measure of the significance. Significances which either (1) indicate that the data is more linear than the surrogates (as for small time delay in Figure 3) and/or (2) are less than 2 standard deviations are set to 0 when performing the average. Our choice of two standard deviations ensures that there is at least a 95% probability that the nonlinearity measures are significant. Panel (c) shows the same thing at the three standard deviation level which ensures over 99% probability that the nonlinearity measure is significant. It should be noted that only the relative value of the integrated significance should be compared over the solar cycle (as the significance may be sharply peaked and average to less than 1). Panel (d) shows occurrences of time delays for different bounds on the significance. We have also displayed the sunspot number in panels a,b, and c for comparison. There is an obvious solar cycle effect. There tend to be minima in significance around the peak in the sunspot number. Maxima in the nonlinearity appear approximately two years prior to minimum sunspot number.

3.2. Cumulant-Based Significance

We performed a similar analysis of K_p using the cumulant-based cost defined earlier. For this particular analysis, we Gaussianized the data and computed surrogate datasets using the CAAFT procedure. We show the same solar maximum as computed with the mutual information measure in Figure 6. In panel (a) we show the cost obtained when cumulants are kept to second order. In panel (b) we show the cost obtained when cumulants are kept to fourth order. Panels (c) and (d) show the cumulant-based significance based on second-order cumulants (S_L) and fourth-order cumulants (S_{NL}), respectively. A second example is shown in Figure 7.

Several features are of interest. First, the linear significance measure shows virtually no difference between the measured data and the surrogate data. This result indicates that the method used to construct the surrogates preserves the underlying linear dynamics in accordance with the null hypothesis. Second, although the fourth-order cost does not track the mean of the surrogates, it does lie for the most part within the spread of the surrogates and therefore, we cannot conclude that there is any indicator of nonlinearity.

On the other hand, for the solar minimum discussed earlier we find a similar indicator of nonlinearity. Figures 8-9 are in the same format as Figure 6 for the years 1994-1996 and 1974-1976. As for the case of solar maximum, the linear cost of the data and surrogates is in excellent agreement. On the other hand, the fourth-order cost reveals a significant difference from the surrogate data. For 1994-1996 the appearance of a broad range of nonlinearity extending up to 75 hours is in accordance with our earlier findings based on the mutual-information statistic shown in Figure 3 although the peak maximum is shifted to longer timescales. For 1974-1976 the peak significance is much sharper, stronger, and peaks around 50 hours as in Figure 4.

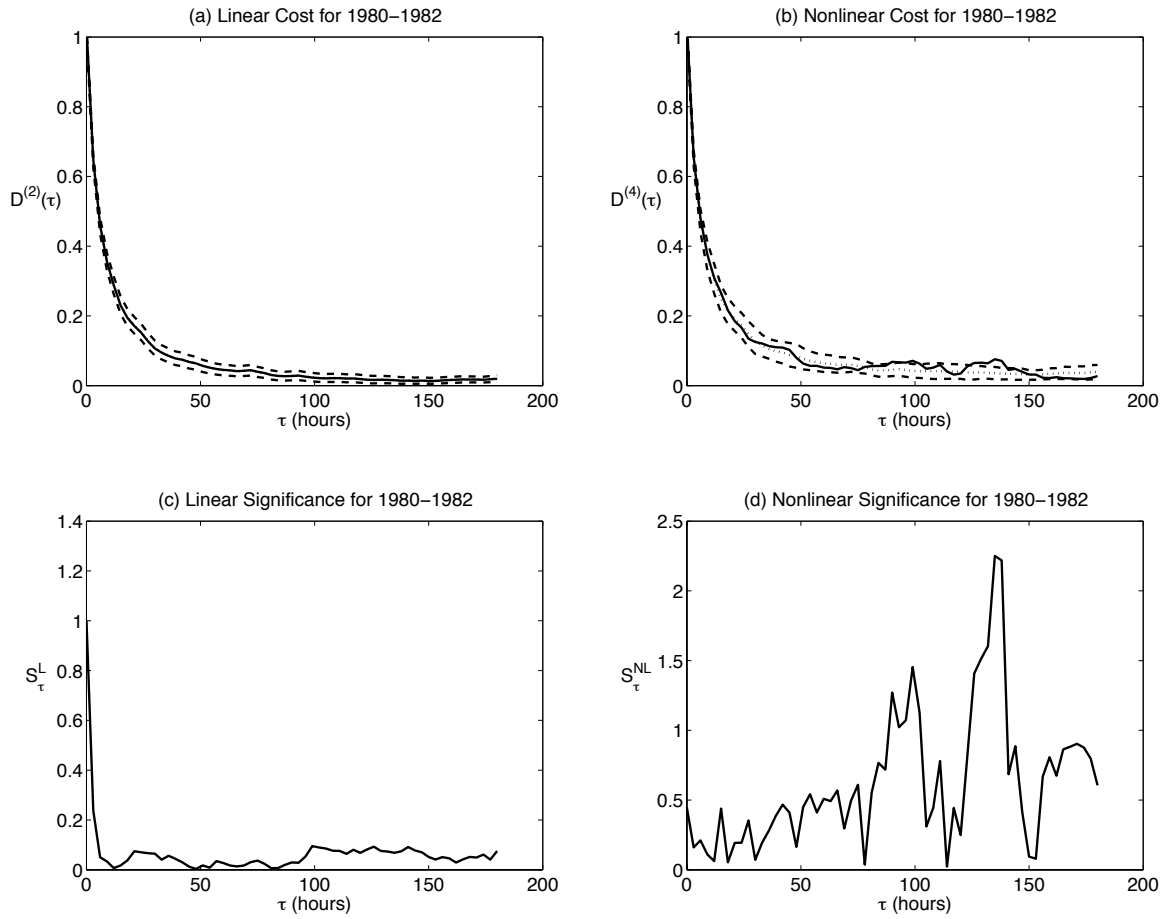

Figure 6. Analysis of K_p data from 1980-1982 (near a solar maximum) using the cumulant-based cost as the discriminating statistic. Panel (a) shows the cost based on keeping cumulants to second order; panel (b) shows the cost based on keeping cumulants to fourth order; panel (c) shows the linear significance (based on panel (a)) and panel (d) shows the nonlinear significance (based on panel (b)). That the surrogate data constructed by the CAAFT method captures the linear properties of the data well is indicated by a linear significance that is generally less than 1. For this data, the nonlinear significance of the actual data does not differ appreciably from the surrogate data. In panel (a) and (b) the mean of the surrogate is shown with a dotted line and the standard deviation are shown as dashed lines.

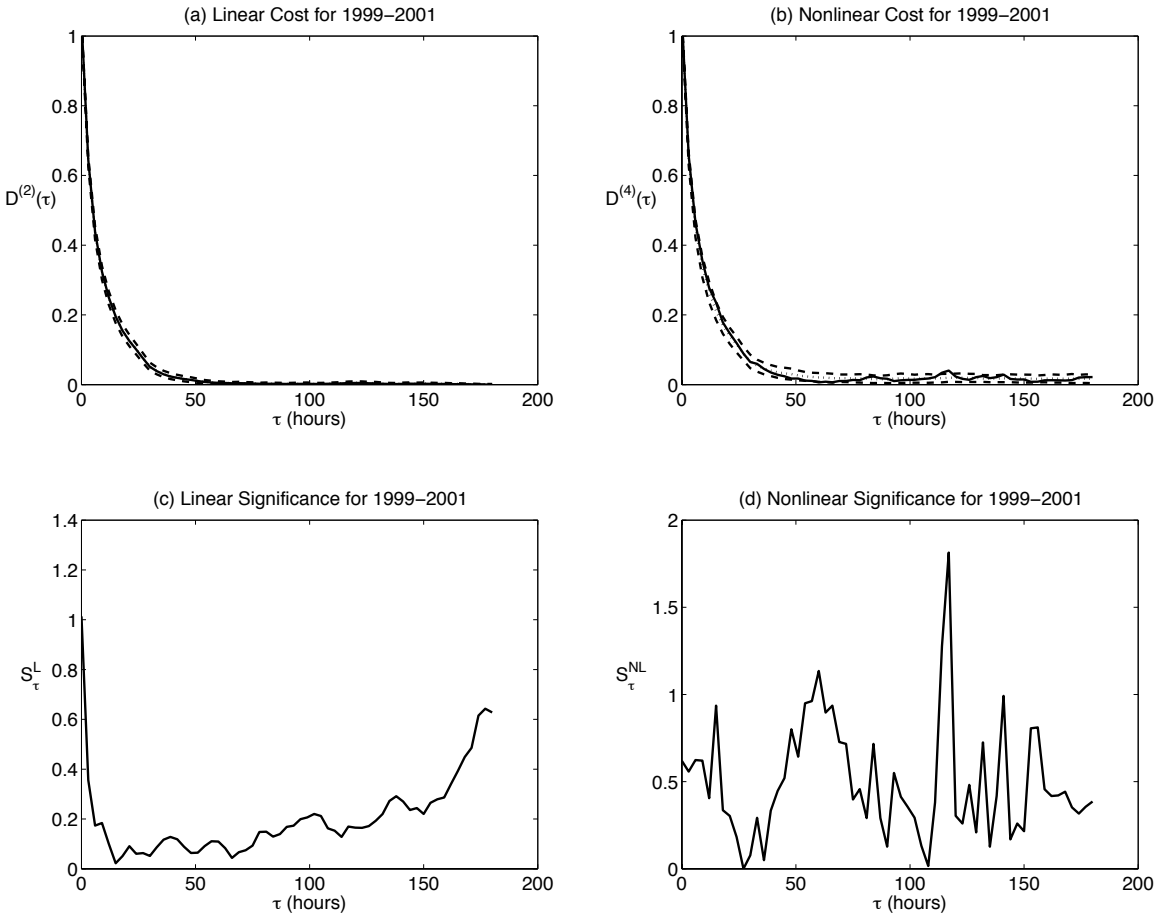

Figure 7. Analysis of K_p data from 1999-2001 (near a solar maximum) using the cumulant-based cost as the discriminating statistic. The format is the same as for Figure 6. Note that as for the 1980-1982 solar maximum, there is no evidence to suggest any difference in the discriminating statistic from the surrogate data which was obtained from the CAAFT method.

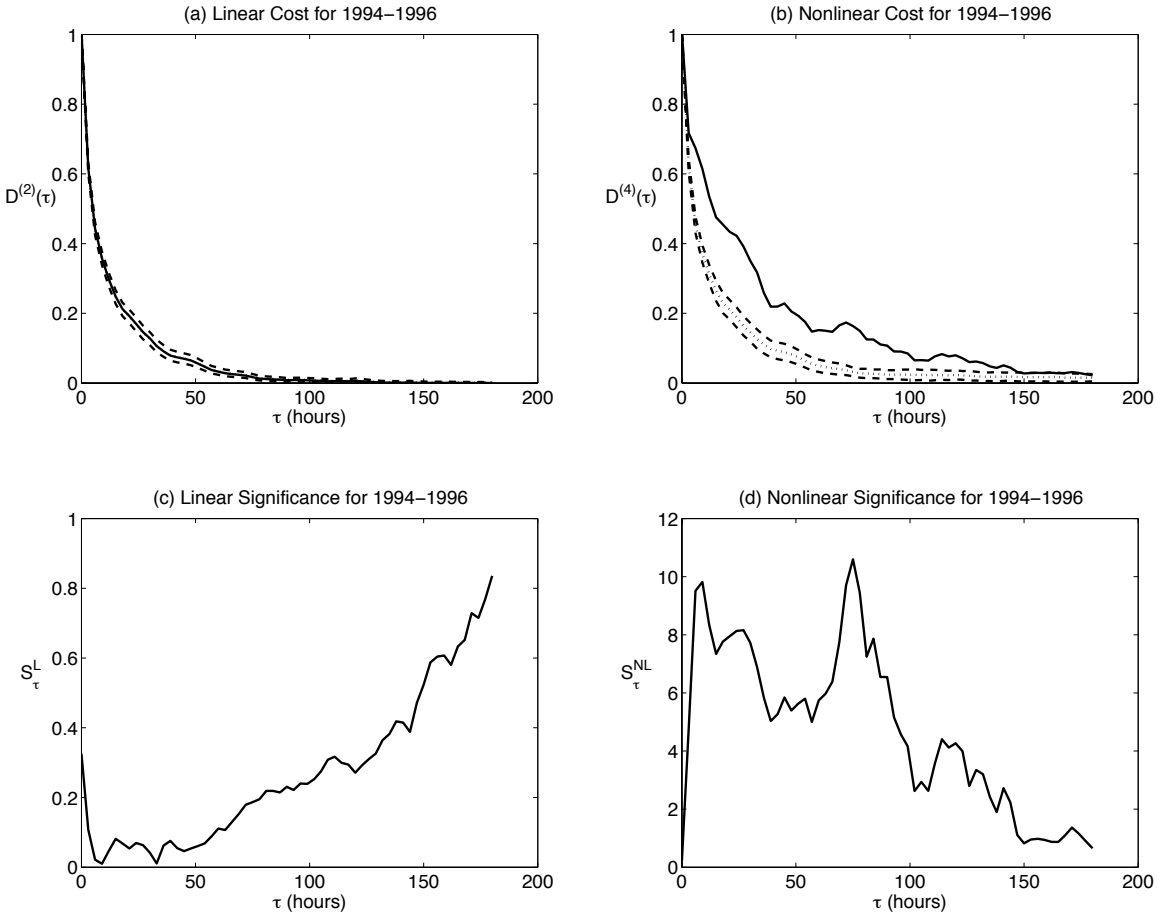

Figure 8. Analysis of K_p data from 1994-1996 (near a solar minimum) using the cumulant-based cost as the discriminating statistic. The format is the same as for Figure 6. Note that although the linear properties of the K_p time series are well reproduced by the surrogates, the discriminating statistic indicates that there is significant nonlinearity that has not been captured. Note that there is a broad range of large significance with a noticeable peak around 75 hours. The broad extent of the large significance is similar to Figure 3 although the maximum significance appears to be shifted to 75 hours.

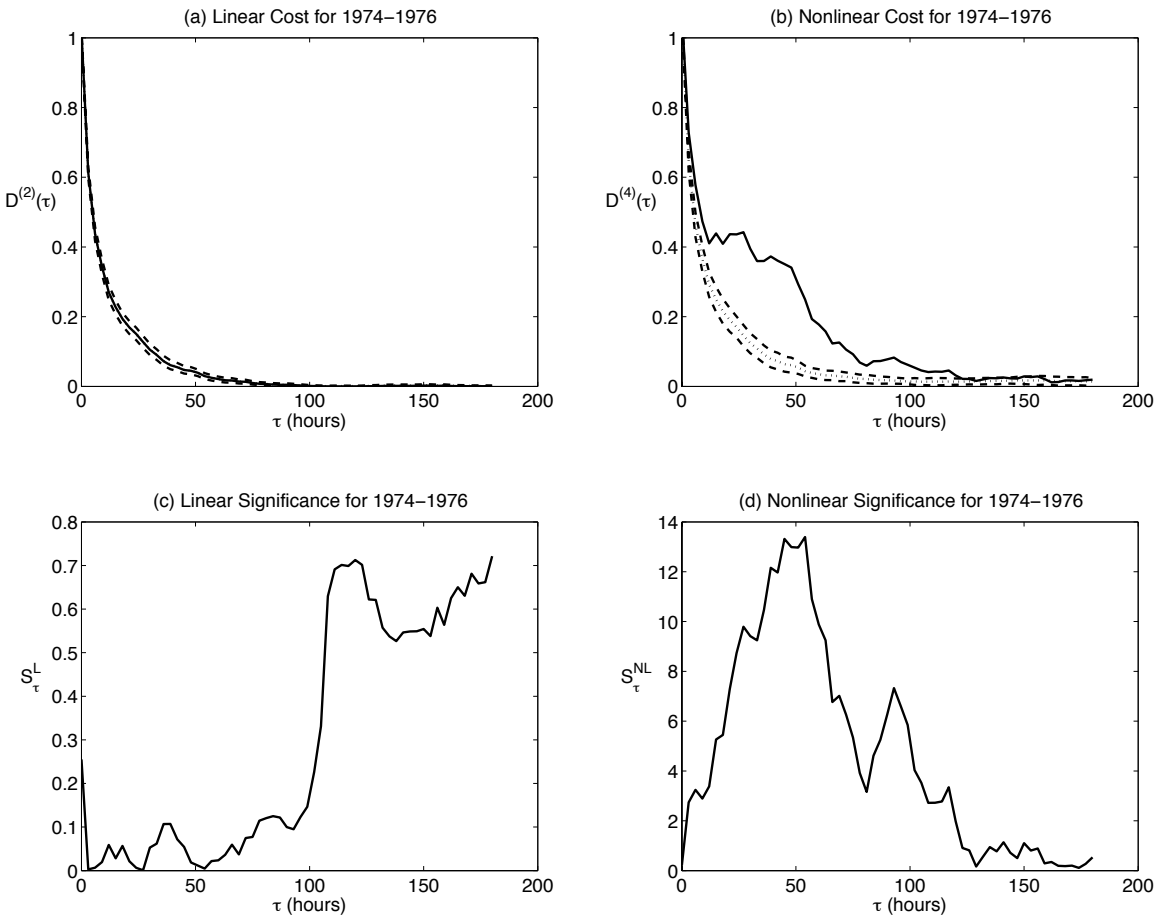

Figure 9. Analysis of K_p data from 1974-1976 (near a solar minimum) using the cumulant-based cost as the discriminating statistic. For this case, the significance is more sharply peaked than for Figure 8 and similar to the significance based on the mutual-information based statistical measure shown in Figure 4.

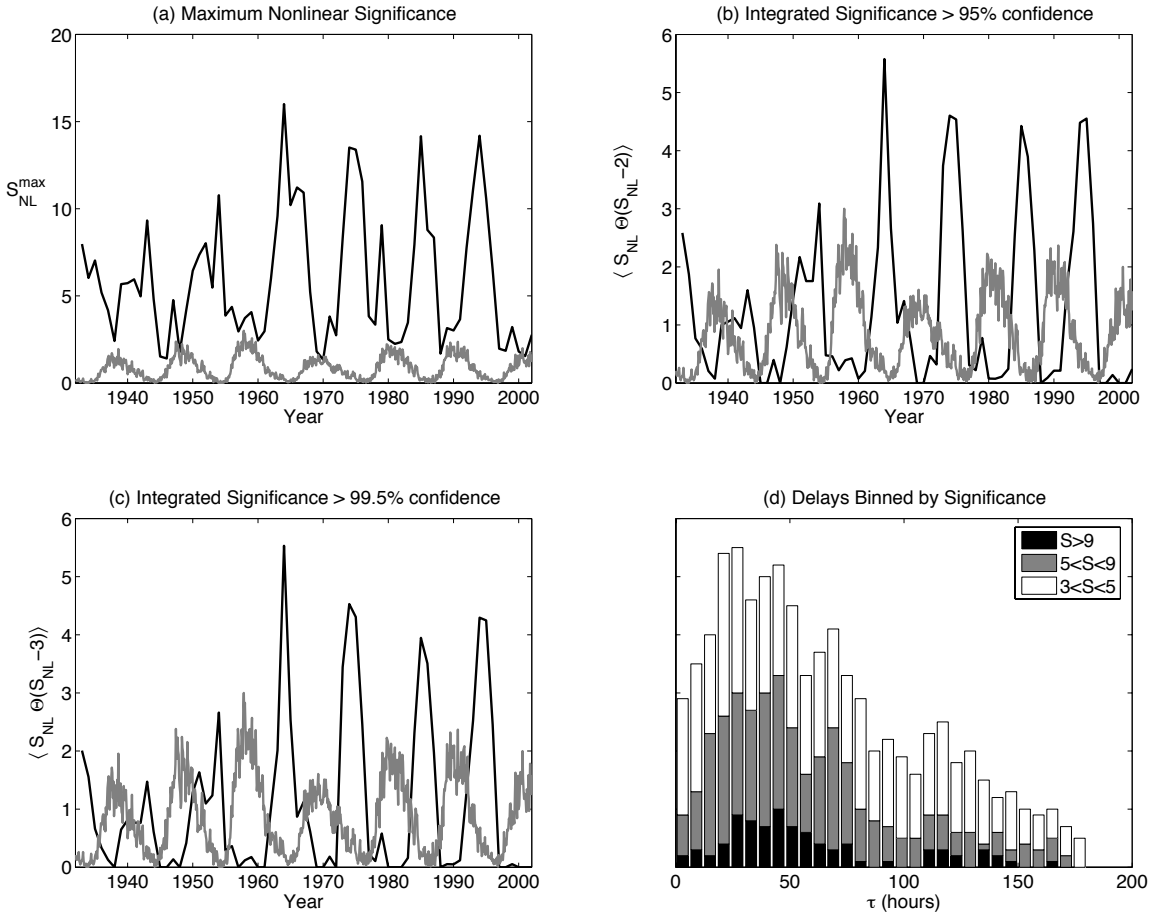

Figure 10. The solar cycle dependence of the cumulant-based nonlinear significance is shown for the historical K_p timeseries. Panel (a) shows the maximum significance for each 3 year window of data; panel (b) integrates all positive significance larger than 2; panel (c) integrates all positive significance larger than 3; and panel (d) shows a histogram of all significance measures larger than 3 for all historical K_p. The data are grouped into several significance ranges. Statistically, the significance peaks around 40-50 hours. When restricted to larger significance events the peaks remain at approximately at the same time delay. For reference, the sunspot number (scaled for clarity) has been shown in panels (a)-(c). Note that minima in the nonlinearity coincide with maximum sunspot number and the maximum nonlinearity occurs approximately two years before the minimum sunspot number.

We also performed an analysis for the years 1932-2003 using the cumulant-based significance as shown in Figure 10. For this case, the solar cycle dependence of the nonlinearity is even more obvious than for the mutual-information based statistic. The peak occurs roughly two years prior to minimum sunspot number. Although the peak significance does vary from solar cycle to solar cycle, within the solar cycle the value of the significance and the time delay remain roughly the same. We also performed a statistic on the occurrences of various time delays binned according to the significance measure. The most significant events appear to have a time-delay around 25-50 hours—although the peak is broad. At higher significance, the peak shifts up to around 50 hours.

3.3. Comparison of M-I and Cumulant Results

Qualitatively, the mutual information approach and the cumulant-based approach present similar results. Figures 1-2 and 6-7 each indicate that for those solar maxima there is no detectable nonlinearity in the data. On the other hand Figures 3-4 and 8-9 each indicate that just prior to solar minimum there is a significant nonlinearity. In comparing Figures 3 and 8 it should be noted that both discriminating statistics indicate a strong broad nonlinearity ranging up to 75 hours with weaker nonlinearity up to 150 hours ($\sim$one week). In contrast, the nonlinearity shown in Figures 4 and 9 is more sharply peaked near 50 hours and is qualitatively similar.

Figures 5 and 10 indicate a solar cycle dependence. The sunspot number is shown in these plots for reference. Maxima and minima in sunspot number are clearly seen in the data for these years with an 11 year period. The solar cycle proceeds in the following manner: just prior to solar minimum a band of sunspots forms at mid-latitude on the solar surface and rapidly reaches a peak in number. The sunspot bands gradually move to lower latitude over the course of the solar cycle and eventually disappear following the emergence of a new band of sunspots at mid-latitude. At the time of solar minimum sunspot bands at both mid- and low-latitude are found. The solar wind plasma also changes character during the solar cycle. Recent satellite observations from Ulysses indicate in the declining phase near solar minimum most of the energy from the solar wind source goes into a steady high speed polar solar wind. The fast flows arise from large coronal holes that cover the polar regions at this time during the solar cycle. At low latitudes, the solar wind is much slower and intermittent [*McComas et al.*, 2000]. On the other hand, during solar maximum, the global 3-D structure of the solar wind is completely different. Near maximum, highly variable flows are observed at all heliolatitudes. These flows arise from a mixture of sources including streamers, coronal mass ejections, and small low latitude coronal holes [*Neugebauer et al.*, 2002].

The maxima of the nonlinear significance occurs just prior to the re-emergence of sunspots at mid-latitude at the time of high speed polar streams. Both the mutual information- and cumulant-based measures show this behavior. The cumulant-based measure seems to yield more uniform results with less variation while the mutual-information based measure seems to have greater variation in the peak amplitudes. The peaks in nonlinearity near 1964 and 1985 appear to be more emphasized with the cumulant-based measure than the mutual-information based measure.

The binned delays also provide an interesting comparison. In both cases, the total distribution of nonlinearity with significance greater than 3 appears to peak around 25-50 hours. However, the mutual information based significance seems to provide a much more sharply peaked distribution than the cumulant-based significance. In both cases, higher significance nonlinear correlations tend to peak around 50 hours.

While there are many similarities in the results, the differences likely rise from the statistical nature of the analysis. In computing the mutual information-based measure, we considered three year windows of data which provided approximately 8760 data points from which to construct the probability distributions. For histogram estimation of the probability distribution function it is proposed that $\log_2 N + 1 + \log_2(1 + \hat{\kappa}\sqrt{N/6})$ is the proper number of bins for histogram estimation where N is the number of data points and $\hat{\kappa}$ is the kurtosis of the data [*Venables and Ripley*, 1994]. This gives 18 data bins which we have found to give the best statistics. Indeed, using the actual binning of K_p into 28 discrete bins provides far noisier statistics and the nonlinearity cannot be identified. The best binning choice also tries to divide the data equally among the bins which tends to wash out features in the higher K_p values. On the other hand, the cumulant-based significance does not require binning of the data as it is based on moments of the distribution. Moreover, we also Gaussianized the data which also provides a cleaner signal for the discriminating statistic. Because the cumulant-base measure is more reliable for limited and noisy datasets, we are inclined

to trust that statistic more than the mutual information where there is a discrepancy between them.

3.4. Is the Nonlinearity Imposed by the Solar Wind?

Having established that there is a nonlinearity in the K_p data, it is natural to ask whether the nonlinearity is intrinsic to the solar wind or whether it is the result of the nonlinear interaction between the solar wind and the magnetosphere. To examine this question, it is useful to examine the solar wind data. It is commonly believed that VB_s and the dynamical pressure are drivers of magnetospheric activity. The history of these variables from Nov 1963 through Nov 1999 has been presented by *Papitashvili et al.* [2000]. In the last two solar cycles, the maxima of VB_s occurred shortly after the peak sunspot number while the minima coincided with minimum sunspot number. The dynamical pressure rises abruptly over one to two years beginning near solar maximum, then slowly decreases until the next solar maximum [*Papitashvili et al.*, 2000; *Richardson et al.*, 2001].

To evaluate the intrinsic nonlinearity in the solar wind, we examine data taken from the WIND satellite. The data has been propagated from the satellite location to the earth and is computed in the GSM coordinate system. Because there is missing data in this time series it is not straightforward to apply the CAAFT method to construct surrogate data. The following procedure was used to construct the surrogate datasets. First, the autocorrelation for the original data set was computed from available data. This procedure only requires pairs of data points separated by time τ which ranges in our calculation up to an arbitrary cutoff. Once the autocorrelation function is computed, we obtain the Fourier transform which is the power spectrum of the original time series. The power spectrum could also be obtained using Fourier techniques developed for unevenly sampled data [*Press et al.*, 1992, section 13.8]. From the power spectrum we take the square root of the Fourier coefficients and multiply by random phases. The inverse Fourier transform then provides surrogate data which is sorted and mapped to the original data set. The surrogate data has the same linear properties as the original data set. The proof of this assertion lies in the comparison of the linear significance of the original data (with its data gaps) and the surrogate data sets.

In Figure 11 we plot the linear and nonlinear cost of the VB_s time series for 1995. When comparing this figure with Figure 8 notice the significant differences in the timescale for the decay of correlations. The magnetosphere requires about twice as long to become decorrelated than the solar wind. Moreover, the nonlinear cost of the magnetosphere decays over a far longer timescale (1 week) compared with the falloff of the solar wind (which basically shows no substantial correlations beyond 2 days). There is a relatively strong nonlinearity in the solar wind detected up to around 25 hours. The nonlinearities at 80 and 180 hours barely rise above the 3 sigma significance compared with the large significance levels seen in the K_p data over the extended period. Moreover, the peaks at large τ are questionable in light of the small value of the cost. The large sigma value occurs because all the surrogates basically show no correlation beyond about 30 hours and therefore the spread of the surrogates is small leading to an overly enhanced significance. The spread in the solar wind data should be contrasted with the spread in the K_p surrogates which remains relatively constant over the entire range of τ.

The dynamic pressure shown in Figure 12 for 1995 has a longer correlation time than VB_s but there is no indication of the existence of nonlinear correlations over the entire range of correlation time considered. It is not readily apparent why the short correlation time nonlinearity of VB_s is not also seen in the dynamical pressure. It should also be noted that because the correlations do not decay so rapidly the spread of surrogates remains reasonably large and no spurious peaks are found at long correlation time.

At solar maximum, basically the same pattern is seen in the solar wind data with strong nonlinearity in VB_s at short correlation time. The absence of any apparent solar cycle nonlinearity that matches the magnetospheric nonlinearity leads us to conclude that the nonlinearity detected in K_p is not the result of an intrinsic nonlinearity in the solar wind that is being filtered by the magnetosphere. It seems more likely that the nonlinearity is the result of the nonlinear interaction between the solar wind and magnetosphere that results from intrinsic nonlinear behavior of the magnetosphere responding to the solar wind driver.

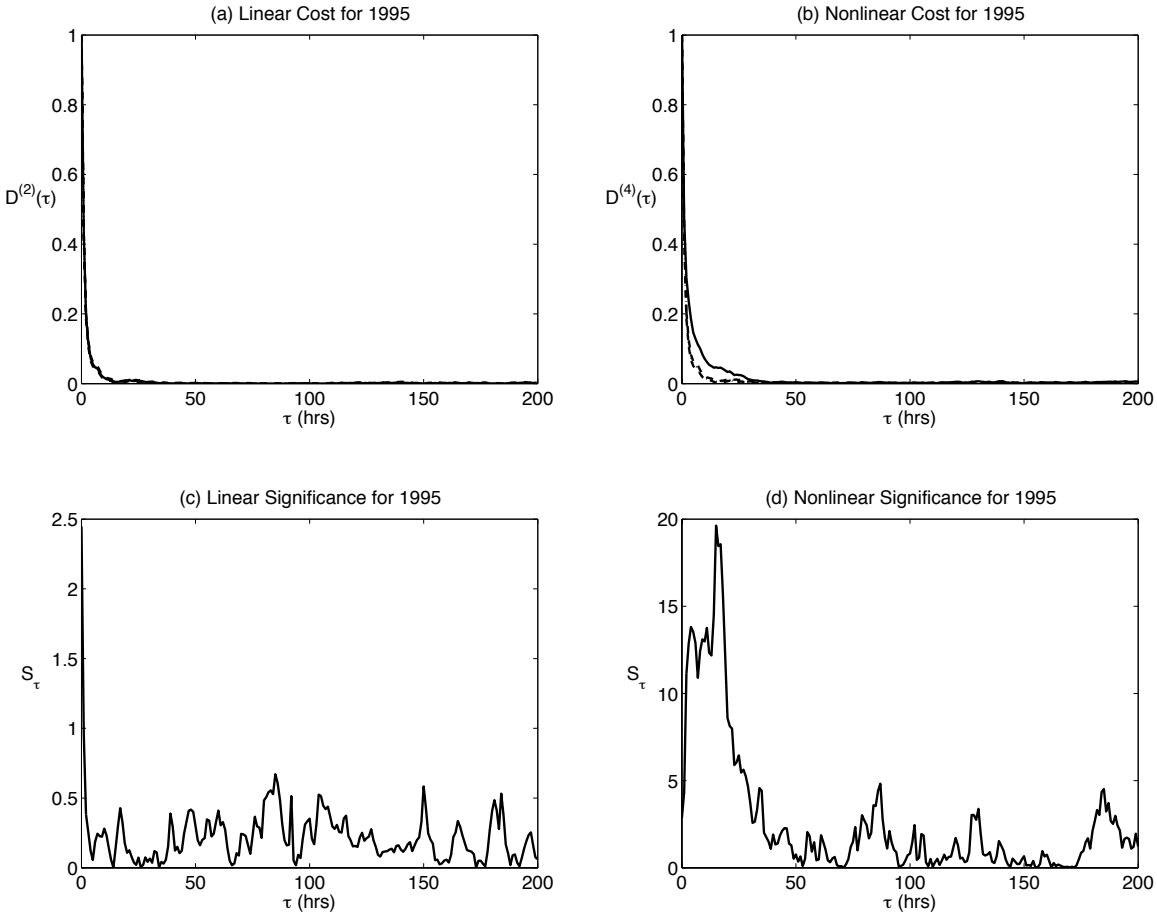

Figure 11. Analysis of VB_s data from 1995 (near a solar minimum) using the cumulant-based cost as the discriminating statistic. Panel (a) shows the linear cost keeping cumulants to second order, panel (b) shows the nonlinear cost keeping cumulants to fourth order, panel (c) shows the linear significance comparing with the surrogate data and panel (d) shows the nonlinear significance. The mean of the surrogate data is shown in dotted and the spread with dashed lines. The main feature is the existence of a nonlinearity at correlation times between 5 and 30 hours.

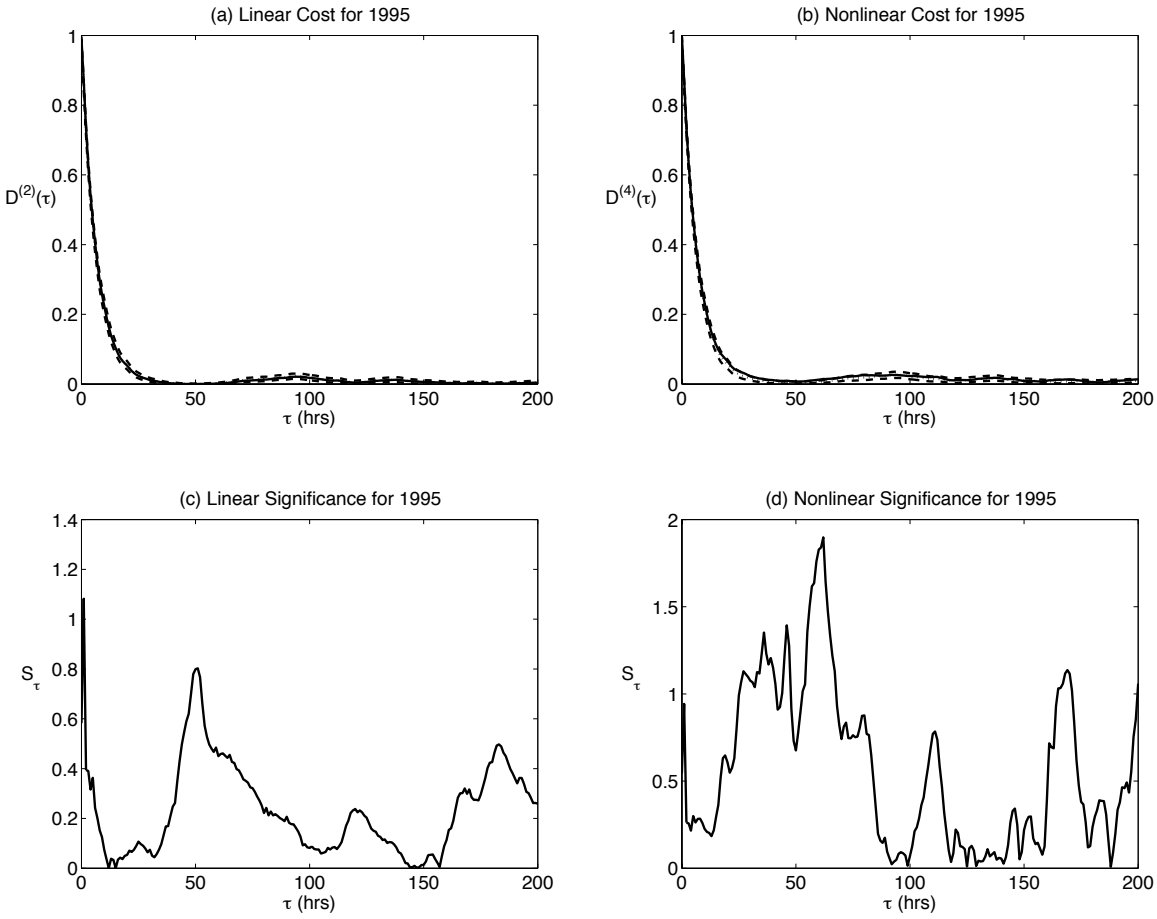

Figure 12. Analysis of dynamic pressure data from 1995 (near a solar minimum) using the cumulant-based cost as the discriminating statistic following the same format of Figure 11. The main feature is the absence of any appreciable nonlinearity. Note that the strong nonlinearity seen in VB_s at small correlation time is absent in the analysis of the dynamical pressure.

3.5. Cross-significance of solar wind and magnetosphere data

So far, we have only considered dependencies between the input and output for single variables (K_p, VB_s, and dynamical pressure). In this section, we generalize the approach to consider the nonlinear correlations between multiple variables. In this case, we are interested in understanding the nonlinear coupling between the solar wind and magnetospheric dynamical systems. *Price and Prichard* [1993] examined a similar question using a variety of statistics and concluded that VB_s and AE exhibited some evidence for deterministic nonlinear response using two different discriminating statistics. We therefore consider coupling between a solar wind variable such as VB_s and K_p. For this comparison, we will consider the contribution to the higher order cumulants for: (a) $\{VB_s(t-\tau), VB_s(t)\}$, (b) $\{K_p(t-\tau), K_p(t)\}$, and (c) $\{VB_s(t-\tau), K_p(t)\}$ as shown in Figure 13. As we have seen previously, the higher order cumulants provide a measure of nonlinearity relative to a set of surrogates. For simplicity, in this analysis, we Gaussianize the variables and construct the surrogates by scrambling the data. We plot difference between the second and fourth order cumulants against the correlation time. The cumulants are normalized to a common factor.

We present our analysis for 1995 in Figure 13, which is near a solar minimum and was examined previously in Figures 8 and 11. The first item to be noted is that the difference between the fourth order cost and second order cost is qualitatively representative of the nonlinear significance when the costs were compared against surrogate data sets. This is the obvious consequence that the surrogate data basically have the same second order cumulant as the original data and the fourth order cumulant statistically vanishes. It is clear that the VB_s nonlinearity has shorter correlation time than the K_p nonlinearity. Moreover, the cross correlation between VB_s and K_p peaks around 3 hours and then tracks the VB_s nonlinearity up to around 25 hours. The peak around 3 hours is similar to timescales obtained from linear prediction filters that are dominated by the linear magnetospheric response [*Bargatze et al.*, 1985]. On the other hand, the nonlinear cross correlation does not appear at all like the K_p nonlinearity which has timescales on the order of 50 hours. This result suggests that the K_p nonlinearity is related to internal magnetospheric dynamics and not to inherent nonlinearity in the solar wind driver.

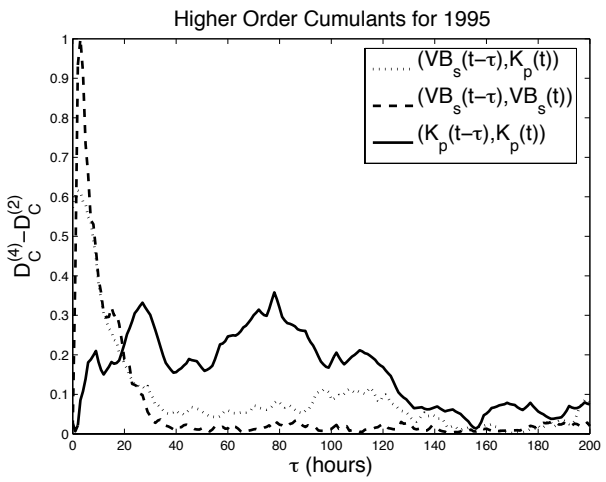

Figure 13. Higher order cumulants obtained from the following input-output pairs: $\{VBs(t), K_p(t-\tau)\}$ (dotted) $\{VBs(t), VBs(t-\tau)\}$ (dashed), and $\{K_p(t), K_p(t-\tau)\}$ (solid) for 1995. The difference between the fourth order cumulant measure and the second order cumulant measure is shown as a function of correlation time, τ. The cumulants are all normalized to a common factor and the reader is referred to Figures 8 and 11 for comparison with surrogate data. Note that the cross correlation between the solar wind VB_s data and K_p tracks the VB_s nonlinearity between 10 hours and 25 hours. On the other hand, the high significance peaks in the K_p nonlinearity do not appear to be related to the intrinsic solar wind nonlinearity. This result suggests that the K_p nonlinearity is the result of internal dynamical behavior of the magnetosphere.

3.6. Solar Cycle Dependence of the Nonlinearity

Our study seems to indicate that the magnetospheric dynamics captured by the K_p index exhibits a nonlinearity. Although the nonlinearity does not appear to be intrinsic to the solar wind, it does appear to be related to the solar cycle as evidenced by the solar cycle dependence of the significance. It is natural to consider whether the nonlinearity may be related to the strength of the solar wind driver, which determines the nonlinear dynamical properties for analogue models of the magnetosphere [e.g. *Klimas et al.*, 1992; *Horton et al.*, 1999].

Due to the strong linear response of the magnetosphere to solar wind drivers [*Bargatze et al.*, 1985; *Vassiliadis et al.*, 2002], it is reasonable to consider

the K_p level as an indicator of the strength of the driver. We performed a linear cross-correlation study comparing the monthly sunspot number with the monthly average of the K_p index since 1932. The results are shown in Figure 14. First, it is apparent that K_p is highly correlated on average with the 11 year solar cycle over the history of the K_p index with a short one or two year lag time. (It should be noted that solar cycle 21 has an unusually large four year lag time). The maximum anti-correlation occurs with a time lag of 6 years indicating that the smallest monthly average K_p tends to occur 6 years following solar maximum (that is, at solar minimum). Although not plotted, the minima and maxima autocorrelation of the sunspot number basically occur at the same lag as the cross correlation of K_p and the sunspot number. This result shows that magnetospheric activity is strongest just following the solar maximum and gradually weakens approaching solar minimum. It seems reasonable to conclude that the primary driver of this activity is strongest around solar maximum and becomes weaker approaching solar minimum.

On the other hand, the cumulant-based significance shown in the dashed curve of Figure 14 appears to be anti-correlated with the sunspot number with a time lag of approximately 4.5 years. The mutual information based significance has a slightly shorter time lag. If the strength of K_p is considered as a proxy for strength of the primary solar wind driver, this result indicates that the primary solar wind driver is not in phase with the nonlinearity detected by the statistical analysis presented in this paper.

As mentioned in §3.3 the appearance of nonlinearity in the descending phase of the solar cycle occurs around the time when high velocity streams are observed at high latitude with respect to the ecliptic plane of the solar system. There is also an increase in solar wind velocity at low latitudes during the descending phase to solar minimum [*Luhmann et al.*, 2002]. It should be noted however that the total ram pressure near the earth (considered to be a primary driver) actually decreases at this time due to an decrease in density [*Richardson et al.*, 2001; *McComas et al.*, 2003]. Because the primary drivers of magnetospheric activity would appear to be decreasing at this time, it seems plausible that the solar wind velocity acts as a secondary driver with increased importance. The solar wind speed is, in fact, believed to have a significant driving effect on magnetospheric activity as evidenced through correlations between the solar

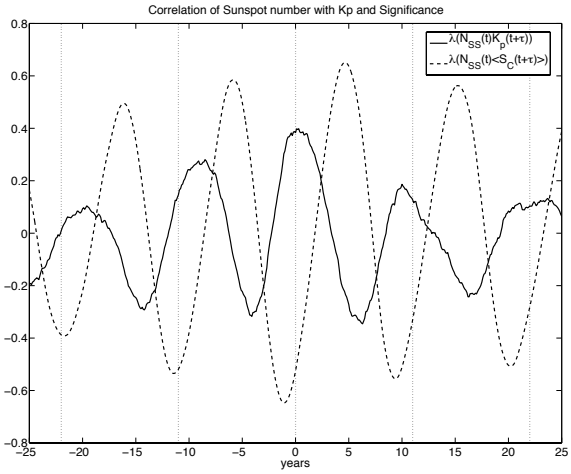

Figure 14. Linear cross correlation, λ of the sunspot number, $N_{SS}(t)$, with $K_p(t+\tau)$ and the cumulant-based integrated significance from Figure 10b as a function of correlation time, τ in years. It is apparent that the K_p index is closely related to the sunspot number while the significance is somewhat anti-correlated. If the K_p index is taken as a proxy for the strength of the magnetospheric driver, it is apparent that the driver follows the solar cycle (maximum at solar maximum and minimum at solar minimum). It should be noted that the maximum significance correlation typically occurs two years prior to solar minimum.

wind speed and electron fluxes in the magnetosphere [*Vassiliadis et al.*, 2002].

To examine the relationship between the solar wind velocity and the nonlinearity detected in the descending phase of the solar cycle, we have examined the relationship between the solar wind speed measured by IMP8 and a measure of nonlinear significance (taken from panel b of Figure 10) in Figure 15a. The average velocity (computed with a 100 day window) is compared with yearly significance computed with a three year sliding window, and it can be seen that the speed and significance are somewhat correlated (although the fact that some features are not correlated does indicate that the relationship may be more complicated). The linear cross-correlation between the mutual information based significance and the solar wind speed demonstrates that they are best correlated with time lag smaller than 1 year (that is, they both peak around the same time during the solar cycle). We therefore conclude that although the nonlinearity is not well correlated with the maximum of K_p activity, it is closely correlated with increased

solar wind speed during the descending phase prior to solar minimum.

This finding raises a number of interesting questions. First, the fact that the nonlinearity detected in our study (Figures 5 and 10) appears to maximize just prior to solar minimum (when the primary driver is weaker) and to minimize around solar maximum (when the primary driver is stronger) seems somewhat counterintuitive. Indeed, studies of the analogue model of *Klimas et al.* [1992] found regular periodic behavior of the model magnetosphere for a weak steady driver, but chaotic model behavior for a strong intermittent driver. The increase of CMEs and solar wind drivers such as VBs and dynamic pressure around solar maximum would seem to be the natural conditions for increased nonlinear behavior. Such nonlinearity was not detected in our analysis.

On the other hand, *Horton et al.* [1999] presented a study of a complex dynamical system known as the WINDMI model for the solar-wind driven magnetosphere-ionosphere system. The solar-wind driving potential was used as a forcing parameter in the model. As forcing was increased the low-state fixed point lost its stability leading to period doubling bifurcations and chaos. However, at stronger forcing, the system eventually returned to stability [*Horton et al.*, 1999]. *Horton et al.* [1999] suggested that the inverse bifurcation corresponded to storm-like magnetospheric states. It may well be that around the time of solar maximum, when the magnetospheric driver is stronger, the system is over-driven and responds more linearly. Such behavior is typical of a driven, damped pendulum. When weakly driven, the pendulum exhibits linear behavior. At larger amplitudes, the pendulum enters a chaotic regime where the dynamics is highly nonlinear. When over-driven the pendulum again exhibits linear behavior.

On the other hand, in the descending phase of the solar cycle just prior to solar minimum, the primary driver is weaker, but the velocity is larger. The increased solar wind velocity appears to be related to a significant nonlinear internal magnetospheric response. We suggest that when the primary solar drivers are large, the magnetosphere locks on to the solar wind and the linear response to the solar wind dominates dominates internal magnetospheric dynamics. In the descending phase of the solar cycle prior to solar minimum, when the magnetosphere is more weakly driven by the solar wind, the internal magnetospheric dynamics related to increased solar wind velocity can play a more important role.

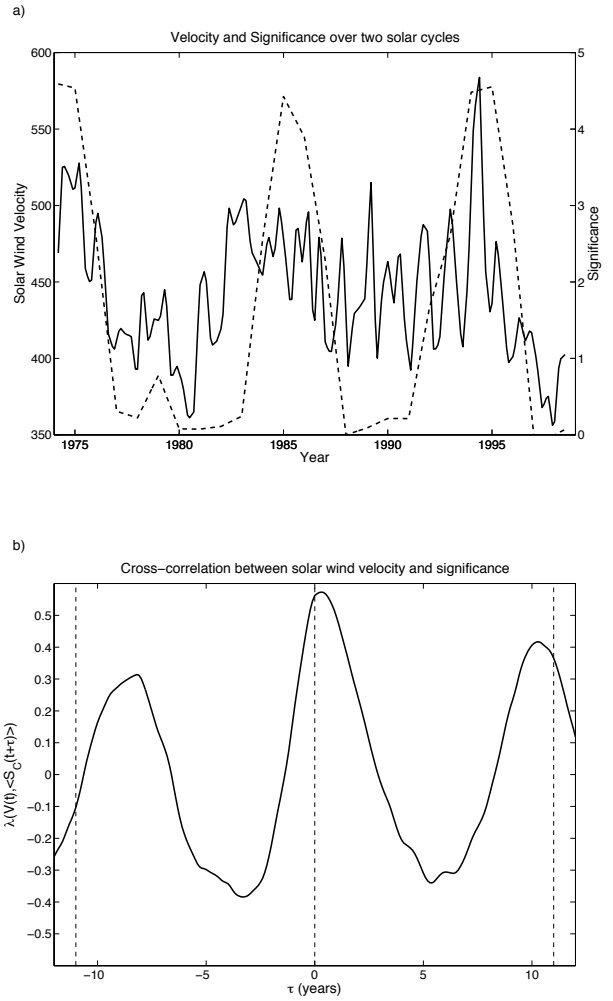

Figure 15. The solar wind speed and the significance obtained in 10b are shown in panel a. The velocity has been averaged over 100 day windows. Panel b shows that the correlation is peaked at zero time delay indicating that the appearance of the nonlinearity is well correlated with the appearance of high speed velocity streams. It should be noted that other variables such as VBs and dynamical pressure are not closely related temporally to the significance.

3.7. Physical Mechanisms Responsible for the Nonlinearity

It is also of interest to identify the physical mechanism responsible for the nonlinear dynamical behavior. The typical timescale for the magnetospheric nonlinearity detected in our analysis is on the order of one to two days. The nonlinearity typically decays away on the order of one week. This timescale is much longer than the coherence time of solar wind drivers or coupling processes related to global geotail Alfvén oscillations (approximately 1 hour) or M-I coupling mediated by Alfvén waves (approximately 10 minutes) [*Horton et al.*, 1999].

On the other hand, the timescales are consistent with relaxation processes that are associated with disturbed magnetospheric events. Recovery from storms typically last up to a week in accordance with the decay of the nonlinear significance. Moreover, the 1-3 day timescale for nonlinear response is well in accordance with relaxation processes that are responsible for recovery of the magnetosphere. A similar analysis of D_{st} data indicates very similar behavior of the nonlinear response with a nonlinear response peaked around 1-2 days. By examining 300 hour windows for the cumulant based significance we also found that large significance typically accompanies large negative excursions of the D_{st} index. These factors suggest that the nonlinear peaks may be associated with recovery of the ring current following storms. Moreover, electron fluxes out to geosynchronous orbit are also observed to be correlated with solar wind speed on the timescale of 1 to 2 days [*Vassiliadis et al.*, 1999].

While the K_p index was not designed to provide the best measure of the ring current, it does respond to changes in the ring current. The ring current at the time of storms is built up through injection of particles from the magnetotail and outflows from the ionosphere. During the recovery phase of storms, the ring current decays due to various loss mechanisms—adiabatic drifts through the dayside magnetopause, charge exchange, wave-particle interactions, Coulomb collisions, and collisions at low altitude with the atmosphere [*Daglis et al.*, 1999; *Jordanova*, 2003, and references therein]. The primary loss mechanism for the storm-time ring current is charge exchange which has a lifetime of hours to days [*Tinsley*, 1976]. An important secondary mechanism is wave particle interactions. *Khazanov et al.* [2002] and *Jordanova* [2003] have shown that wave growth of electromagnetic ion cyclotron waves near the He^+ and O^+ cyclotron frequencies can also be a significant source of ion loss due to wave-particle scattering into the loss cone. Such waves are typically excited by temperature anisotropies that develop as the result of (a) compression of the magnetosphere and (b) differences in gradient and curvature drift as a function of pitch angle. The timescale for EMIC induced proton diffusion is 0.8, 4.3, and 48 days for EMIC amplitudes of 0.1, 0.035, and 0.01 nT [*Albert*, 2003]. EMIC waves in the equatorial region are commonly found with amplitudes as large as 1 nT [*Labelle and Treumann*, 1992]. It should be noted that oxygen, hydrogen, and helium decays may be somewhat different leading to multiple-phase decays as well.

3.8. Relevance of Nonlinearity to K_p Predictive Models

The existence of significant nonlinearity in K_p dynamics due to internal magnetospheric dynamics could potentially complicate predictability of magnetospheric dynamics based on solar wind input. The importance of this internal response has been recognized and included in empirical predictive models [*Burton et al.*, 1975] and has also been incorporated into neural network models using recurrent neural networks which allows for a nonlinear memory capacity [*Wu and Lundstedt*, 1996, 1997].

In the context of our statistics-based findings it is interesting to consider the results of the Costello neural network [*Costello*, 1997, http://www.sec.noaa.gov/rpc/costello/index.html] which is purely driven by the solar wind inputs: V,IMF $|B|$, and IMF B_z. We examined the performance of the Costello neural network over the course of two solar cycles (1975-2001). The model was evaluated by comparing the neural network predictions with the data using the skill scores defined in [*Detman and Joselyn*, 1999] and the results are shown in Figure 16. Although the results are fairly accurate during quiet times ($K_p<5$), they are less accurate during moderate or active times ($K_p>5$). This behavior is also consistent with the previous evaluation of Costello model [Detman and Joselyn, 1999]. The correlation coefficient between the forecast and official Kp is 0.75.

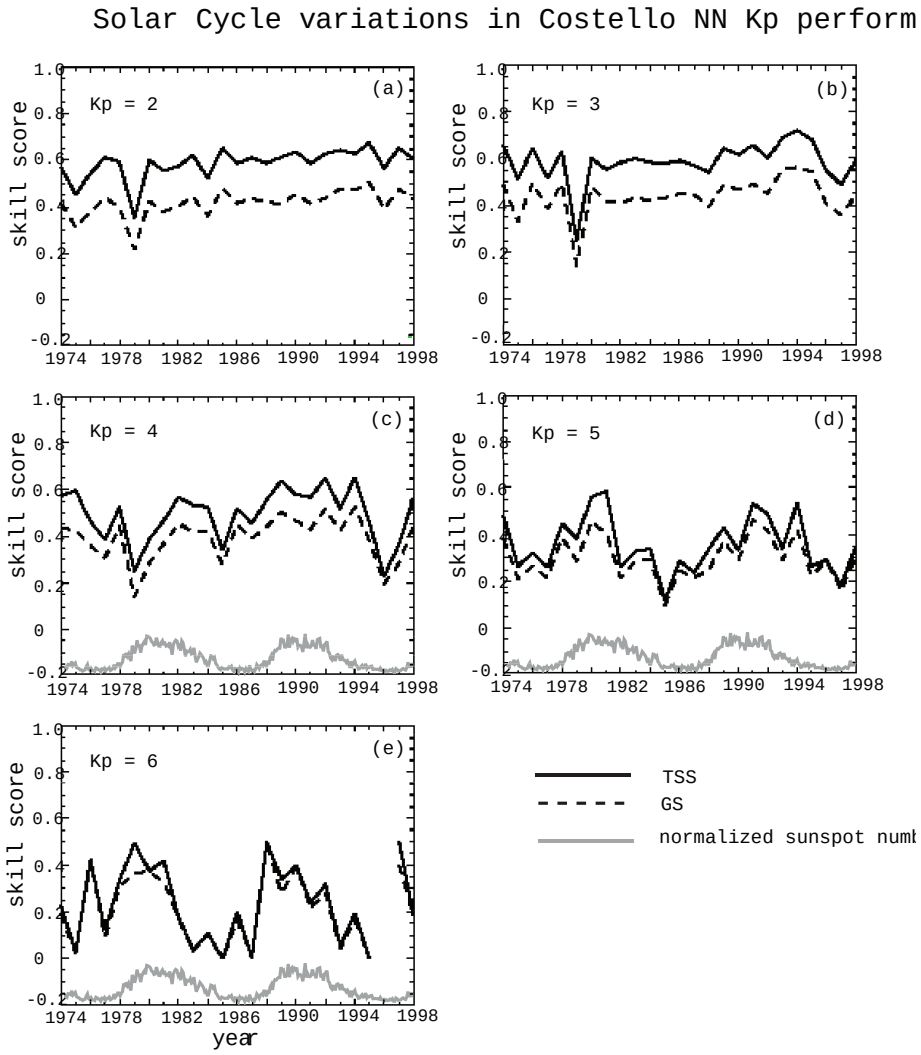

Figure 16. Performance of the Costello NN over two solar cycles from 1974 to 1998. The True Skill Statistic (TSS) and Gilbert Skill (GS) scores have the following interpretation: a value of 1 indicates a perfect forecast, a value of 0 indicates a random forecast, and negative values can also indicate anti-correlation between the forecast and the data. The results indicate that the Costello network could use improvement—especially for active conditions. Moreover, the variation of the scores over the solar cycle indicates that the neural network performs much better at solar maximum than at solar minimum. This result is not surprising given our finding that the dynamics involve more nonlinearity at solar minimum.

The most interesting feature of this plot is that there is better predictability at solar maximum than at solar minimum. This result is consistent with our findings that the system behaves more linearly at solar maximum than at solar minimum. One would expect that a more linear system would have better predictability. In a companion paper, *Wing et al.* [2004] have analyzed four neural network predictors of K_p, and found that the network trained with solar wind data spanning two solar cycles also exhibits this same solar cycle dependence. *Wing et al.* [2004] have also shown that keeping past history of K_p improves predictability for short term forecasts and significantly reduces this solar cycle dependence. This result suggests that an internal response may be necessary to capture the nonlinear relaxation of the magnetosphere during solar minimum.

4. Conclusions

In this paper we have introduced two discriminating statistics that can be used to detect the presence of nonlinear correlations in a multivariate system. Our analysis of the K_p data indicates that the dynamics of the K_p variable may be captured statistically with a linear AR model at solar maximum, while a few years prior to solar minimum when sunspots first appear at mid-latitude, the K_p variable exhibits a significant nonlinearity. This nonlinearity appeared regularly during the course of seven solar cycles spanned by the K_p dataset. The nonlinearity seems to peak around 30-50 hours and gradually decreases over the course of a one week correlation time. The highest significance nonlinear correlations seem to have a timescale on the order of 50 hours.

The overall timescale of the nonlinearity (on the order of a week) is the same time associated with recovery from storms. The peak timescale, 1-2 days, seems to be a timescale associated with charge exchange and wave-particle interactions associated with ring current relaxation.

Our examination of the solar wind data seems to indicate a that the intrinsic nonlinearity of the solar wind variables has a much smaller correlation time that vanish rapidly compared with the long correlation time of the K_p index. Therefore, it is reasonable to conclude that the nonlinearity is not the result of the magnetosphere filtering an intrinsic solar wind nonlinearity, but rather that the nonlinearity results from the internal dynamical response to different solar wind drivers.

Although magnetospheric activity is strongest shortly after solar maximum, the nonlinearity is not detected at that time. The absence of nonlinearity may be related to the fact that the system is strongly driven and the linear magnetospheric response to the driver suppresses the internal magnetospheric nonlinearity. On the other hand, when the magnetospheric activity is smaller around solar minimum, the internal magnetospheric nonlinearity is detected and internal dynamics are more important. The nonlinearity appears to be closely associated with increased solar wind speed. Solar wind speed is also correlated with electron flux levels on the same timescale as the nonlinearity detected in our analysis [*Vassiliadis et al.*, 2002]. These results seems consistent with the finding that the Costello neural network model shows greater predictability of K_p at solar maximum (most linear) than at solar minimum (most nonlinear) when only external drivers are considered.

Acknowledgments The authors would like to thank J. Freeman for sharing the Costello NN code with us. This work was supported by NASA Grant NAG5-10971, NSF Grant ATM-9819705, NASA Grant W-19880, NSF Grant ATM-0218847, and DoE Contract No. DE-AC02-76-CHO-3073. Dr. Johnson thanks Sorin Zaharia for useful discussions.

References

Albert, J. M., Evaluation of quasi-linear diffusion coefficients for EMIC waves in a multispecies plasma, *Journal of Geophysical Research (Space Physics)*, *108*(A6), 16–1, 2003.

Baker, D. N., R. D. Zwickl, S. J. Bame, E. W. Hones, B. T. Tsurutani, E. J. Smith, and S.-I. Akasofu, An ISEE 3 high time resolution study of interplanetary parameter correlations with magnetospheric activity, *J. Geophys. Res.*, *88*(17), 6230–6242, 1983.

Bargatze, L. F., D. N. Baker, E. W. Hones, and R. L. McPherron, Magnetospheric impulse response for many levels of geomagnetic activity, *J. Geophys. Res.*, *90*, 6387–6394, 1985.

Burton, R. K., R. L. McPherron, and C. T. Russell, An emperical relationship between interplanetary conditions and Dst, *J. Geophys. Res.*, *80*, 4204–4214, 1975.

Clauer, C. R., R. L. McPherron, C. Searls, and M. G. Kivelson, Solar wind control of auroral zone geo-

magnetic activity, *Geophys. Res. Lett.*, *8*, 915–918, 1981.

Costello, K. A., Moving the rice msfm into a real-time forecast mode using solar wind driven forecast models, Ph.D. thesis, Rice University, Houston, TX, 1997.

Crooker, N. U., and K. I. Gringauz, On the low correlation between long-term averages of solar wind speed and geomagnetic activity after 1976, *J. Geophys. Res.*, *98*(17), 59–62, 1993.

Daglis, I. A., R. M. Thorne, W. Baumjohann, and S. Orsini, The terrestrial ring current: Origin, formation, and decay, *Reviews of Geophysics*, *37*, 407–438, 1999.

Darbellay, G. A., and I. Vajda, Estimation of the Information by an Adaptive Partitioning of the Observations Space, *IEEE Transactions on Information Theory*, *45*, 1315–1321, 1999.

Deco, G., and B. Schürmann, *Information Dynamics*. Springer, 2000.

Detman, T., and J. A. Joselyn, Real-time Kp predictions from ACE real time solar wind, in *Solar Wind Nine*, edited by S. R. Habbal, R. Esser, J. V. Hollweg, and P. A. Isenberg, pp. 729–732. The American Institute of Physics, 1-56396-865-7, 1999.

Gershenfeld, N., *The Nature of Mathematical Modeling*. Cambridge University Press, Cambridge, chapter, 1998.

Gleisner, H., and H. Lundstedt, Response of the auroral electrojets to the solar wind modeled with neural networks, *J. Geophys. Res.*, *102*, 14269–14278, 1997.

Horton, W., and I. Doxas, A low-dimensional energy-conserving state space model for substorm dynamics, *J. Geophys. Res.*, *101*, 27223–27238, 1996.

Horton, W., J. P. Smith, R. Weigel, C. Crabtree, I. Doxas, B. Goode, and J. Cary, The solar-wind driven magnetosphere-ionosphere as a complex dynamical system, *Physics of Plasmas*, *6*, 4178–4184, 1999.

Jordanova, V. K., New Insights on Geomagnetic Storms from Model Simulations Using Multi-Spacecraft Data, *Space Science Reviews*, *107*, 157–165, 2003.

Kennel, M. B., and S. Isabelle, Method to dinstinguish possible chaos from colored noise and to determine embedding parameters, *Phys. Rev. A*, *46*, 3111, 1992.

Khazanov, G. V., K. V. Gamayunov, V. K. Jordanova, and E. N. Krivorutsky, A self-consistent model of the interacting ring current ions and electromagnetic ion cyclotron waves, initial results: Waves and precipitating fluxes, *Journal of Geophysical Research (Space Physics)*, *107*(A6), 14–1, 2002.

Klimas, A. J., D. N. Baker, D. A. Roberts, D. H. Fairfield, and J. Buechner, A nonlinear dynamical analogue model of geomagnetic activity, *J. Geophys. Res.*, *97*, 12253–+, 1992.

Klimas, A. J., D. N. Baker, D. Vassiliadis, and D. A. Roberts, Substorm recurrence during steady and variable solar wind driving: Evidence for a normal mode in the unloading dynamics of the magnetosphere, *J. Geophys. Res.*, *99*, 14855–14862, 1994.

Kugiumtzis, D., Surrogate Data Test for Nonlinearity Including Non-Monotonic Transforms, *Physical Review E*, *62*, 25–28, 1999.

Labelle, J., and R. A. Treumann, Poynting vector measurements of electromagnetic ion cyclotron waves in the plasmasphere, *J. Geophys. Res.*, *97*(16), 13789–+, 1992.

Li, W., Mutual Information Functions Versus Correlation Functions, *J. Stat. Phys.*, *60*, 823–837, 1990.

Luhmann, J. G., Y. Li, C. N. Arge, P. R. Gazis, and R. Ulrich, Solar cycle changes in coronal holes and space weather cycles, *Journal of Geophysical Research (Space Physics)*, *107*, 3–1, 2002.

McComas, D. J., et al., Solar wind observations over Ulysses' first full polar orbit, *J. Geophys. Res.*, pp. 10419–10434, 2000.

McComas, D. J., H. A. Elliott, N. A. Schwadron, J. T. Gosling, R. M. Skoug, and B. E. Goldstein, The three-dimensional solar wind around solar maximum, *Geophys. Res. Lett.*, *30*, 24–1, 2003.

Neugebauer, M., P. C. Liewer, E. J. Smith, R. M. Skoug, and T. H. Zurbuchen, Sources of the solar wind at solar activity maximum, *Journal of Geophysical Research (Space Physics)*, *107*, 13–1, 2002.

Papitashvili, V. O., N. E. Papitashvili, and J. H. King, Solar cycle effects in planetary geomagnetic activity: Analysis of 36-year long OMNI dataset, *Geophys. Res. Lett.*, *27*, 2797–2800, 2000.

Press, W. H., S. A. Teukolsky, W. T. Vetterling, and B. P. Flannery, *Numerical Recipies*. Cambrige University Press, 1992.

Price, C. P., and D. Prichard, The non-linear response of the magnetosphere - 30 October 1978, *Geophys. Res. Lett.*, *20*, 771–774, 1993.

Prichard, D., and C. Price, Spurious dimension estimates from time series of geomagnetic indices, *Geophys. Res. Lett.*, *19*, 1623–1626, 1992.

Prichard, D., and C. P. Price, Is the AE index the result of nonlinear dynamics?, *Geophys. Res. Lett.*, *20*, 2817–2820, 1993.

Richardson, J. D., C. Wang, and K. I. Paularena, The solar wind: from solar minimum to solar maximum, *Advances in Space Research*, *27*, 471–479, 2001.

Roberts, D. A., Is there a strange attractor in the magnetosphere?, *J. Geophys. Res.*, *96*(15), 16031–+, 1991.

Roberts, D. A., D. N. Baker, A. J. Klimas, and L. F. Bargatze, Indications of low dimensionality in magnetospheric dynamics, *Geophys. Res. Lett.*, *18*, 151–154, 1991.

Schreiber, T., and A. Schmitz, Improved surrogate data for nonlinearity tests, *Phys. Rev. Lett.*, *77*, 635–639, 1996.

Sharma, A. S., D. Vassiliadis, and K. Papadopoulos, Reconstruction of low-dimensional magnetospheric dynamics by singular spectrum analysis, *Geophys. Res. Lett.*, *20*, 335–338, 1993.

Takens, F., Detecting strange attractors in turbulence., in *Dynamical Systems and Turbulence*, edited by D. A. Rand, and L. S. Young, vol. 898 of *Lecture Notes in Mathematics*, p. 366. Springer-Verlag, 1980.

Theiler, J., S. Eubank, A. Longtin, B. Galdrikian, and J. Doyne Farmer, Testing for nonlinearity in time series: the method of surrogate data, *Physica D Nonlinear Phenomena*, *58*, 77–94, 1992.

Tinsley, B. A., Evidence that the recovery phase ring current consists of helium ions, *jgr*, *81*(10), 6193–6196, 1976.

Tsonis, A. A., Probing the linearity and nonlinearity in the transitions of the atmospheric circulation, *Nonlinear Processes in Geophysics*, *8*, 341–345, 2001.

Ukhorskiy, A. Y., M. I. Sitnov, A. S. Sharma, and K. Papadopoulos, Global and multiscale aspects of magnetospheric dynamics in local-linear filters, *Journal of Geophysical Research (Space Physics)*, *107*, 15–1, 2002.

Vassiliadis, D., A. S. Sharma, and K. Papadopoulos, Lyapunov exponent of magnetospheric activity from AL time series, *Geophys. Res. Lett.*, *18*, 1643–1646, 1991.

Vassiliadis, D., A. J. Klimas, D. N. Baker, and D. A. Roberts, A description of the solar wind-magnetosphere coupling based on nonlinear filters, *J. Geophys. Res.*, *100*, 3495–3512, 1995.

Vassiliadis, D., A. J. Klimas, J. A. Valdivia, and D. N. Baker, The D_{st} geomagnetic response as a function of storm phase and amplitude and the solar wind electric field, *J. Geophys. Res.*, *104*, 24957–24976, 1999.

Vassiliadis, D., A. J. Klimas, S. G. Kanekal, D. N. Baker, and R. S. Weigel, Long-term-average, solar cycle, and seasonal response of magnetospheric energetic electrons to the solar wind speed, *Journal of Geophysical Research (Space Physics)*, *107*, 22–1, 2002.

Vassiliadis, D. V., A. S. Sharma, T. E. Eastman, and K. Papadopoulos, Low-dimensional chaos in magnetospheric activity from AE time series, *Geophys. Res. Lett.*, *17*, 1841–1844, 1990.

Venables, W. N., and B. D. Ripley, *Modern Applied Statistics with S-Plus*. Springer, New York, 1994.

Wing, S., J. Jen, J. R. Johnson, C.-I. Meng, D. G. Sibeck, K. Bechtold, J. Freeman, K. Costello, and M. Balikhin, Kp Forecast Models, submitted to *Journal of Geophysical Research*, 2004.

Wu, J., and H. Lundstedt, Prediction of geomagnetic storms from solar wind data using Elman recurrent neural networks, *Geophys. Res. Lett.*, *23*, 319–322, 1996.

Wu, J., and H. Lundstedt, Neural network modeling of solar wind-magnetosphere interaction, *J. Geophys. Res.*, *102*, 14457–14466, 1997.

This preprint was prepared with the AGU LaTeX macros v3.0. File CUMpp formatted 2005 January 19.

With the extension package 'AGU++', version 1.2 from 1995/01/12

External Distribution

Plasma Research Laboratory, Australian National University, Australia

Professor I.R. Jones, Flinders University, Australia

Professor João Canalle, Instituto de Fisica DEQ/IF - UERJ, Brazil

Mr. Gerson O. Ludwig, Instituto Nacional de Pesquisas, Brazil

Dr. P.H. Sakanaka, Instituto Fisica, Brazil

The Librarian, Culham Science Center, England

Mrs. S.A. Hutchinson, JET Library, England

Professor M.N. Bussac, Ecole Polytechnique, France

Librarian, Max-Planck-Institut für Plasmaphysik, Germany

Jolan Moldvai, Reports Library, Hungarian Academy of Sciences, Central Research Institute for Physics, Hungary

Dr. P. Kaw, Institute for Plasma Research, India

Ms. P.J. Pathak, Librarian, Institute for Plasma Research, India

Dr. Pandji Triadyaksa, Fakultas MIPA Universitas Diponegoro, Indonesia

Professor Sami Cuperman, Plasma Physics Group, Tel Aviv University, Israel

Ms. Clelia De Palo, Associazione EURATOM-ENEA, Italy

Dr. G. Grosso, Instituto di Fisica del Plasma, Italy

Librarian, Naka Fusion Research Establishment, JAERI, Japan

Library, Laboratory for Complex Energy Processes, Institute for Advanced Study, Kyoto University, Japan

Research Information Center, National Institute for Fusion Science, Japan

Dr. O. Mitarai, Kyushu Tokai University, Japan

Dr. Jiangang Li, Institute of Plasma Physics, Chinese Academy of Sciences, People's Republic of China

Professor Yuping Huo, School of Physical Science and Technology, People's Republic of China

Library, Academia Sinica, Institute of Plasma Physics, People's Republic of China

Librarian, Institute of Physics, Chinese Academy of Sciences, People's Republic of China

Dr. S. Mirnov, TRINITI, Troitsk, Russian Federation, Russia

Dr. V.S. Strelkov, Kurchatov Institute, Russian Federation, Russia

Professor Peter Lukac, Katedra Fyziky Plazmy MFF UK, Mlynska dolina F-2, Komenskeho Univerzita, SK-842 15 Bratislava, Slovakia

Dr. G.S. Lee, Korea Basic Science Institute, South Korea

Dr. Rasulkhozha S. Sharafiddinov, Theoretical Physics Division, Insitute of Nuclear Physics, Uzbekistan

Institute for Plasma Research, University of Maryland, USA

Librarian, Fusion Energy Division, Oak Ridge National Laboratory, USA

Librarian, Institute of Fusion Studies, University of Texas, USA

Librarian, Magnetic Fusion Program, Lawrence Livermore National Laboratory, USA

Library, General Atomics, USA

Plasma Physics Group, Fusion Energy Research Program, University of California at San Diego, USA

Plasma Physics Library, Columbia University, USA

Alkesh Punjabi, Center for Fusion Research and Training, Hampton University, USA

Dr. W.M. Stacey, Fusion Research Center, Georgia Institute of Technology, USA

Dr. John Willis, U.S. Department of Energy, Office of Fusion Energy Sciences, USA

Mr. Paul H. Wright, Indianapolis, Indiana, USA

The Princeton Plasma Physics Laboratory is operated
by Princeton University under contract
with the U.S. Department of Energy.

Information Services
Princeton Plasma Physics Laboratory
P.O. Box 451
Princeton, NJ 08543

Phone: 609-243-2750
Fax: 609-243-2751
e-mail: pppl_info@pppl.gov
Internet Address: http://www.pppl.gov